
AFRL-RX-WP-TM-2010-4085

# COLLABORATIVE RESEARCH AND DEVELOPMENT (CR&D)

## Delivery Order 0043: Deformation and Texture Development During Hot Working of Titanium

**A.A. Salem**

**Universal Technology Corporation**

**M.G. Glavicic**

**UES, Inc.**

**S.L. Semiatin**

**Metals Branch**
**Metals, Ceramics, & NDE Division**

**APRIL 2008**
**Final Report**



**AIR FORCE RESEARCH LABORATORY**
**MATERIALS AND MANUFACTURING DIRECTORATE**
**WRIGHT-PATTERSON AIR FORCE BASE, OH 45433-7750**
**AIR FORCE MATERIEL COMMAND**
**UNITED STATES AIR FORCE**

# NOTICE AND SIGNATURE PAGE

Using Government drawings, specifications, or other data included in this document for any purpose other than Government procurement does not in any way obligate the U.S. Government. The fact that the Government formulated or supplied the drawings, specifications, or other data does not license the holder or any other person or corporation; or convey any rights or permission to manufacture, use, or sell any patented invention that may relate to them.

This report was cleared for public release by the USAF 88th Air Base Wing (88 ABW) Public Affairs Office (PAO) and is available to the general public, including foreign nationals. Copies may be obtained from the Defense Technical Information Center (DTIC) (http://www.dtic.mil).

AFRL-RX-WP-TM-2010-4085 HAS BEEN REVIEWED AND IS APPROVED FOR PUBLICATION IN ACCORDANCE WITH THE ASSIGNED DISTRIBUTION STATEMENT.

| | |
|---|---|
| *//Signature// | //Signature// |
| RITA SCHOLES<br>Project Manager<br>Business Operations Branch<br>Integration and Operations Division<br>Materials and Manufacturing Directorate | ROBERT ENGHAUSER<br>Acting Chief<br>Business Operations Branch<br>Integration and Operations Division |

This report is published in the interest of scientific and technical information exchange, and its publication does not constitute the Government's approval or disapproval of its ideas or findings.

*Disseminated copies will show "//Signature//" stamped or typed above the signature blocks.

# REPORT DOCUMENTATION PAGE

*Form Approved*
*OMB No. 0704-0188*



| 1. REPORT DATE *(DD-MM-YY)* | 2. REPORT TYPE | 3. DATES COVERED *(From - To)* |
|---|---|---|
| April 2008 | Final | 03 November 2005 – 31 January 2008 |

**4. TITLE AND SUBTITLE**
COLLABORATIVE RESEARCH AND DEVELOPMENT (CR&D)
Delivery Order 0043: Deformation and Texture Development During Hot Working of Titanium

**5a. CONTRACT NUMBER**
F33615-03-D-5801-0043

**5b. GRANT NUMBER**

**5c. PROGRAM ELEMENT NUMBER**
61202F

**6. AUTHOR(S)**
A.A. Salem (Universal Technology Corporation)
M.G. Glavicic (UES, Inc.)
S.L. Semiatin (AFRL/RXLM)

**5d. PROJECT NUMBER**
4349

**5e. TASK NUMBER**
L0

**5f. WORK UNIT NUMBER**
4349L0VT

**7. PERFORMING ORGANIZATION NAME(S) AND ADDRESS(ES)**

| | | |
|---|---|---|
| Universal Technology Corporation<br>1270 North Fairfield Road<br>Dayton, OH 45432-2600 | UES, Inc.<br>4401 Dayton-Xenia Road<br>Dayton, OH 45433 | Metals Branch (AFRL/RXLM)<br>Metals, Ceramics, & NDE Division<br>Air Force Research Laboratory<br>Materials and Manufacturing Directorate<br>WPAFB, OH 45433-7750<br>Air Force Materiel Command<br>United States Air Force |

**8. PERFORMING ORGANIZATION REPORT NUMBER**
S-531-043

**9. SPONSORING/MONITORING AGENCY NAME(S) AND ADDRESS(ES)**
Air Force Research Laboratory
Materials and Manufacturing Directorate
Wright-Patterson Air Force Base, OH 45433-7750
Air Force Materiel Command
United States Air Force

**10. SPONSORING/MONITORING AGENCY ACRONYM(S)**
AFRL/RXOB

**11. SPONSORING/MONITORING AGENCY REPORT NUMBER(S)**
AFRL-RX-WP-TM-2010-4085

**12. DISTRIBUTION/AVAILABILITY STATEMENT**
Approved for public release; distribution unlimited.

**13. SUPPLEMENTARY NOTES**
PAO Case Number: 88ABW 2009-0049; Clearance Date: 01 Feb 2009. Report contains color.

Three reports in the subject area of deformation and texture development during hot working of titanium are included.

**14. ABSTRACT**
This research in support of the Air Force Research Laboratory Materials and Manufacturing Directorate was conducted at Wright-Patterson AFB, Ohio from 3 November 2005 through 31 January 2008. This task developed constitutive models for alpha/beta titanium alloys with colony-alpha microstructure and validated texture prediction models for plate rolling. A method for separating the textures of primary alpha ($\alpha_p$) and secondary alpha ($\alpha_s$) in alpha/beta titanium alloys with a duplex microstructure was developed. Utilizing electron backscatter diffraction (EBSD) and energy-dispersive spectroscopy (EDS), the approach relies on the non-uniform partitioning of alloying elements between primary alpha and regions containing secondary-alpha lamellae and residual beta matrix phase. The method was evaluated using samples of Ti-6Al-4V for which vanadium partitions strongly to secondary alpha + beta regions. The technique thus provides a useful tool for quantifying the evolution of *deformation* texture in the primary alpha and *transformation* texture in secondary alpha formed via decomposition of the beta matrix following hot working or final heat treatment.

**15. SUBJECT TERMS**
Titanium, Texture, EBSD, Microstructure, EDS

| 16. SECURITY CLASSIFICATION OF: | | | 17. LIMITATION OF ABSTRACT: | 18. NUMBER OF PAGES | 19a. NAME OF RESPONSIBLE PERSON (Monitor) |
|---|---|---|---|---|---|
| a. REPORT | b. ABSTRACT | c. THIS PAGE | | | Rita Scholes |
| Unclassified | Unclassified | Unclassified | SAR | 64 | 19b. TELEPHONE NUMBER *(Include Area Code)*<br>N/A |

**Standard Form 298 (Rev. 8-98)**
Prescribed by ANSI Std. Z39-18

**CR&D Task Order 43**

**Deformation and Texture Development During Hot Working of Titanium**

Objective: To determine constitutive models for alpha/beta titanium alloys with a colony-alpha microstructure and validate texture prediction models for plate rolling.

Textures of hot rolled Ti-6Al-4V plate with a bimodal were measured and investigated using a texture separation technique based on combining EBSD/EDS systems. The measured texture was explained by the activity of different deformation mechanism. The activity of deformation mechanisms and constitutive behavior of Ti-6Al-4V with a colony-alpha microstructure were determined via laboratory experiments at hot-working temperatures on single-colony samples with orientations chosen to activate hard/soft basal slip (i.e., $a_1$, $a_2$, or $a_3$ slip activation), hard/soft prism slip (i.e., $a_1$, $a_2$, or $a_3$ slip activation), or pyramidal slip (c+a slip activation). Tests included (1) simple compression (single-slip behavior). The load-stroke data were reduced to obtain flow-stress/constitutive relations.

The work is summarized in the following three papers that were submitted for publication. The first paper (Page 1) reported a technique to separate the texture of secondary alpha and primary alpha phases using EBSD/EDS technique. The second paper (Page 13) utilized the texture separation technique to evaluate texture evolution during hot rolling of polycolony Ti-6Al-4V plate with bimodal microstructure at different rolling temperature. The third paper (Page 24) determined the critical resolved shear stresses and slip systems activities during hot working of Ti-6Al-4V single colonies.

# A coupled EBSD/EDS method to determine the primary- and secondary-alpha textures in titanium alloys with duplex microstructures

A.A. Salem[a*], M.G. Glavicic[b], and S.L. Semiatin
Air Force Research Laboratory, Materials and Manufacturing Directorate,
AFRL/MLLM, Wright-Patterson AFB, OH 45433
[a]Universal Technology Corp., 1270 N. Fairfield Road, Dayton, OH 45432
[b]UES Inc., 4401 Dayton-Xenia Road, Dayton, OH 45433

## Abstract

A method for separating the textures of primary alpha ($\alpha_p$) and secondary alpha ($\alpha_s$) in alpha/beta titanium alloys with a duplex microstructure was developed. Utilizing electron backscatter diffraction (EBSD) and energy-dispersive spectroscopy (EDS), the approach relies on the non-uniform partitioning of alloying elements between primary alpha and regions containing secondary-alpha lamellae and residual beta matrix phase. The method was evaluated using samples of Ti-6Al-4V for which vanadium partitions strongly to secondary alpha + beta regions. The technique thus provides a useful tool for quantifying the evolution of *deformation* texture in the primary alpha and *transformation* texture in secondary alpha formed via decomposition of the beta matrix following hot working or final heat treatment.

*Keywords:* titanium, texture, EBSD, microstructure, EDS

## Acknowledgements

This work was conducted as part of the in-house research activities of the Metals Processing Group of the Air Force Research Laboratory's Materials and Manufacturing Directorate. The support and encouragement of the Laboratory management and the Air Force Office of Scientific Research (Dr. B.P. Conner, program manager) are gratefully acknowledged. The assistance of R. Wheeler in conducting the experimental work is much appreciated. Two of the authors were supported through Air Force Contracts F33615-03-D-5801 (AAS) and FA8650-04-D-5235 (MGG).

* Corresponding author (e-mail: ayman.salem@wpafb.af.mil)

## 1.0 INTRODUCTION

Titanium and its alloys are used extensively in the aerospace industry due to their high strength-to-weight ratio, excellent fracture toughness, and good corrosion/oxidation resistance. The allotropic transformation of titanium provides the foundation for the control of microstructure and thus properties via a plethora of thermomechanical processes. Irrespective of the process, however, the overall goal is to control the volume fraction and morphology of the low-temperature alpha (hcp) and high-temperature beta (bcc) phases.

For applications limited by strength, ductility, and/or high-cycle fatigue properties, a duplex structure of primary (globular) alpha ($\alpha_p$) in a transformed-beta matrix (comprising secondary-alpha ($\alpha_s$) lamellae in the continuous beta matrix) is desirable. Such a structure is usually obtained via an ingot-metallurgy approach comprising hot working in the high-temperature beta field followed by a small increment of alpha/beta hot work, recrystallization of the worked beta grains in the beta field, rapid cooling from the beta field to formed a colony microstructure within the prior-beta grains, and, finally, a second alpha/beta hot-working step to convert the lamellar microstructure thus formed into an equiaxed-alpha morphology [1]. More specifically, the second alpha/beta hot working operation gives rise to a structure (at the hot-working temperature) of $\alpha_p$ particles in a matrix of beta which contains residual dislocation substructure. At room temperature, the exact form of the matrix phase depends on the cooling rate following hot working (or subsequent alpha/beta heat treatment) and thus the nature of the decomposition of the metastable beta-matrix phase. If the material is slow cooled from hot working (or heat treatment), $\alpha_s$ lamellae (with a colony morphology) are formed; rapid cooling gives rise to martensitic alpha laths.

Increasing attention is now being focused on the formulation of physics-based models of microstructure/texture evolution and the resulting first- and second-tier mechanical properties. For alpha/beta titanium alloys with a duplex microstructure, for example, methods to determine the individual textures of $\alpha_p$ and $\alpha_s$ are required for the validation of deformation and transformation texture models, respectively. Because the crystal structure and lattice parameters of primary and secondary alpha are identical, conventional x-ray or electron backscatter diffraction (EBSD) techniques can not be applied directly for this purpose. The objective of the current work, therefore, was to formulate and validate an EBSD-based technique for separating the individual textures. This approach was based on the concurrent measurement of local texture and composition using electron backscatter diffraction (EBSD) and energy-dispersive spectroscopy (EDS), respectively. The local composition variation enabled the automated binning of texture readings from the two different micro-constituents.

## 2.0 BACKGROUND

To put the current work into proper context, previously-developed techniques to separate the textures of $\alpha_p$ and $\alpha_s$ in alpha/beta titanium alloys are summarized in this section. For the most part, these prior methods have typically been indirect and consisted of the following steps: (i) measurement of the overall (primary + secondary) alpha texture using x-ray diffraction, neutron diffraction, or EBSD [2], (ii) determination of microstructure by optical or scanning-electron microscopy and separating primary and secondary alpha in the micrographs, (iii) correlating the specific regions for which microstructure and texture have been measured, and (iv) partitioning the texture data based on the difference in morphology of the primary and secondary alpha. In the duplex microstructure, the $\alpha_p$ phase usually comprises equiaxed/globular particles, and $\alpha_s$ are thin lamellae. When using scanning-electron microscope (SEM), the phases are readily distinguished using secondary-electron (SE) or backscattered-electron (BSE) imaging (Figure 1a, b). When using BSE imaging on a polished section, the $\alpha_p$ and $\alpha_s$ both appear dark (due to atomic-number, or Z, contrast). The individual alpha lamellae in the $\alpha_s$ are surrounded by layers of beta (or very fine martensitic alpha) which appear white (or gray) due to enrichment by beta stabilizers (such as vanadium or molybdenum) typically leading to a higher overall Z. Such a contrast between $\alpha_p$ and $\alpha_s$+$\beta$ can be revealed only under low magnification conditions and/or when the $\alpha_s$ lamellae are thin (Figure 1b).

Several different methods have been proposed to distinguish between primary and secondary alpha in micrographs and thus to correlate microstructural features and texture data [3-6]. For instance, Germain, *et al.* [3, 4] linked local orientations determined by the EBSD technique to corresponding positions in BSE images for Ti-6Al-4V. At *low* magnifications (at which the $\alpha_s$ lamellae and the beta matrix are difficult to resolve), $\alpha_p$ appears darker than $\alpha_s$ (Figure 1b). The apparently lighter (gray) level of the $\alpha_s$ results from the averaging effect at low magnification of low-Z secondary alpha and high-Z beta phase enriched in vanadium. The Germain, *et al.* technique is thus limited to low magnification BSE images in microstructures with very fine $\alpha_s$ lamellae. Hence, this approach may be difficult to apply for duplex microstructures with thick $\alpha_s$ lamellae (Figure 1c) or characterization using high magnification BSE images. Moreover, the technique also requires image rotation, resizing, translation, and shearing to match BSE images to EBSD inverse-pole-figure maps. Special software is required for the matching procedure due to differences in acquisition techniques.

Using a similar technique, Thomas, *et al.* [5] correlated EBSD texture information and microstructural information from *optical* images of the same area (e.g., Figure 1d). In this approach, the texture is measured first using EBSD. The sample is then etched to locate and photograph the previously-scanned ("blank") area. Because of the difference in acquisition techniques for texture and microstructure, special software was developed and applied to match EBSD maps and optical micrographs using rotation and resizing. Beside the time needed to etch samples and search for the scanned (blank) area, high resolution scans (step size < 0.5 μm, each with an acquisition time > 0.5 s) are required to produce enough carbon contamination to locate the blank after the etching. Therefore, characterization of a large area to obtain reasonable texture statistics may require long scans, fiducial marks for locating purposes, and extensive manual intervention. In addition, the process is very sensitive to etching time; i.e., the marks left by the scanning process are lost if the etching time is too long.

To overcome some of shortcomings of other methods, Glavicic, *et al.* [6] suggested an indirect technique involving a heat treatment to eliminate the $\alpha_s$ phase. In this approach, x-ray diffraction is used to measure the total ($\alpha_p + \alpha_s$) texture of the duplex microstructure (Figure 2a). The separate $\alpha_p$ texture is then determined on a portion of the sample which has been solution treated at a temperature high enough in the two-phase field to dissolve the $\alpha_s$ and slow cooled to promote growth of the primary alpha without decomposition of the beta matrix (e.g., Figure 2b). The texture of the $\alpha_p$ (weighted by its volume fraction in the initial duplex microstructure) is then subtracted from the $\alpha_p + \alpha_s$ texture. The major shortcoming of this method concerns the implicit assumption that the heat treatment used to obtain the microstructure with only $\alpha_p$ particles maintains the original texture of this phase; in other words, it is assumed that there is (a) no recrystallization or (b) preferential growth of particles with either different amounts of stored work from prior hot working operations or different texture components.

## 3.0 MATERIAL AND EXPERIMENTAL PROCEDURES

The present method to separate the textures of primary and secondary alpha was developed to overcome the shortcomings of earlier techniques. In brief, the approach is based on simultaneous, *in-situ* measurements of local orientation *and* composition within an SEM and eliminates the need for additional heat treatments or special post-processing software. Specifically, Kikuchi patterns and local composition data for the alpha phase are collected automatically inside an SEM using EBSD and energy-dispersive spectroscopy (EDS) detectors, respectively, for each point on the sample surface scanned by the electron beam. For this purpose, it is critical that both detectors be located on the same side of the microscope chamber (facing the surface of the sample), thus ensuring that both measurements are synchronized and come from the same material point during the scanning process. Texture is determined by off-line indexing of the Kikuchi patterns using OIM® data-analysis software [7].

### 3.1 Material

Ti-6Al-4V was used to establish the usefulness of the new experimental technique for separating the textures of primary and secondary alpha, $\alpha_p$ and $\alpha_s$, respectively. The as-received material comprised a 32-mm-thick plate having a measured composition (in weight pct.) of 6.15 aluminum, 3.9 vanadium, 0.20 oxygen, 0.21 iron, 0.008 nitrogen, 0.01 carbon, 0.0031 hydrogen, and balance titanium.

### 3.2 Experimental procedures

To establish baseline microstructure and texture data, the Ti-6Al-4V program material was heated to 955°C for 4 hours (to dissolve all $\alpha_s$ lamellae from prior processing) and then either water quenched (to preserve the $\alpha_p$ texture at 955°C) or furnace cooled to grow a microstructure comprising solely $\alpha_p$ particles.

Preforms of the heat-treated-and-furnace-cooled material were hot rolled at 955°C to a 3:1 reduction (effective strain of 1.15) followed by air cooling. To determine microstructures and textures, samples of the *unrolled* materials and the hot-rolled plate were sectioned along the midplane, ground, and lightly electropolished at –20°C in a solution of 590 ml methanol and 60 ml perchloric acid. Following electropolishing, each sample was mounted on the tilting stage inside an XL30 field-emission-gun scanning-electron-microscope (FEG-SEM). The microscope was operated at 20 kV and 7 nA with the stage tilted at an inclination of 70°. The EDS detector was fully retracted to avoid overexposure due to the large current used to collect the EBSD data.

Local Kikuchi patterns and chemical composition were collected using EBSD and EDS systems from EDAX [7]. A 0.3-μm step size at 50 sec/frame was used to cover an area measuring 80 μm x 120 μm. Different step sizes and larger areas (within the maximum of 25 mm x 50 mm associated with the microscope construction) were also utilized.

The texture results from the present technique were compared to those obtained using the x-ray diffraction (XRD) approach developed previously by Glavicic, *et al.* [6]. For this purpose, an additional sample was removed from the hot-rolled Ti-6Al-4V plate. The piece was cut into two equal sections. One half was analyzed in the as-hot-rolled condition (Figure 2a). The other was given a heat treatment to produce an alpha microstructure that was fully globular (Figure 2b); i.e., it was annealed at 960°C (just above the rolling temperature) for one hour followed by furnace cooling. The volume fraction of primary alpha in the as-hot-rolled duplex microstructure

was determined by analysis of BSE micrographs (Figure 2a) taken in a Leica-Cambridge Stereoscan 360 FEG-SEM. Subsequently, both pieces were prepared for XRD on the RD-TD plane (at the midplane) of the rolled plate using standard metallographic techniques. XRD measurements were conducted using Cu K$\alpha$ radiation from an 18 kW rotating anode source, and textures were determined from measurements of partial (10**Error! Objects cannot be created from editing field codes.**0), (0002), (10**Error! Objects cannot be created from editing field codes.**1), (10**Error! Objects cannot be created from editing field codes.**1), and (11**Error! Objects cannot be created from editing field codes.**0) alpha-phase pole figures. In addition, partial (110) and (200) beta-phase pole figures were determined to enable a comparison of the $\alpha_s$ texture and the texture of the parent beta phase. The partial pole figures were completed using the orientation-distribution-function (ODF) analysis software in popLA (preferred orientation package from Los Alamos National Laboratory) [8].

## 4.0 RESULTS AND DISCUSSION

### 4.1 Microstructure observations for hot-rolled Ti-6Al-4V

Secondary-electron (SE) images revealed that the microstructure of the hot rolled Ti-6Al-4V sample consisted of 60 pct. $\alpha_p$ particles within a matrix comprising colonies of $\alpha_s$ lamellae separated by thin layers of the beta phase (Figure 3a). The shape of the $\alpha_p$ particles was noticeably different from that of the $\alpha_s$ lamellae. On a lightly etched surface, $\alpha_p$ appeared relatively equiaxed; $\alpha_s$ comprised lamellae stacked in bundles.

Observations based on the EBSD data shed additional insight into the nature of the microstructure. In particular, an inverse-pole-figure (IPF) map (Figure 3b) for the same area as the SE image revealed the orientations of the primary and secondary alpha phases. The misorientations across $\alpha_s$ lamellae (using the point-to-point method [7]) within a given colony were smaller than 3°. Hence, each $\alpha_s$ bundle was recognized as a single grain by the OIM® software, and a single color was assigned to all lamellae in the specific colony with no separating boundary. Based on the grain morphologies deduced from IPF maps alone, therefore, it was difficult to distinguish between $\alpha_p$ particles and $\alpha_s$ colonies. Furthermore, backscattered-electron (BSE) images (Figure 1c, 2a) and image-quality maps (Figure 3c) did not show a clear contrast between $\alpha_p$ and $\alpha_s$ as well, thus preventing the application of the technique of Germain, *et al.* [3, 4].

### 4.2 Composition (EDS) results for hot-rolled Ti-6Al-4V

EDS results for the hot-rolled Ti-6Al-4V sample quantified the aluminum and vanadium concentration in different parts of the microstructure. In all cases, a high level of an alloying element was assigned a light color, and a lower level was represented with a darker color. The EDS map for aluminum (Figure 3d) showed a measurable variation in concentration. A comparison between aluminum EDS maps and SE images for the same areas confirmed that the lighter areas belonged to $\alpha_p$ particles and darker areas to $\alpha_s$ lamellae. Specifically, higher aluminum concentrations (i.e., lighter colors) were found for $\alpha_p$ particles, and lower concentrations for $\alpha_s$ lamellae (Figure 3d). Better contrast between $\alpha_p$ and $\alpha_s$ lamellae was revealed in EDS maps for vanadium, however (Figure 3e). The darker areas (lower vanadium) were associated with $\alpha_p$ particles, and lighter areas with $\alpha_s$ lamellae.

The qualitative EDS observations (Figures 3d,e) for the partitioning of alloying elements were as expected based on the phase equilibria determined by Semiatin, *et al.* [9] and Castro and Seraphin [10] for Ti-6Al-4V. In these previous efforts, it was shown that vanadium partitions preferentially to the beta phase between the alpha lamellae, and aluminum partitions preferentially to alpha. The partitioning is especially marked for vanadium; vanadium levels in the alpha and beta phases are of the order of 2 and 15 weight pct., respectively. The EDS measurements for $\alpha_s$ regions are biased by the beta layers, which are enriched in vanadium and depleted in aluminum, thereby giving rise to the observed contrast.

Concentration histograms provided an automated means of separating regions of primary and secondary alpha (Figure 4). The aluminum concentration histogram (Figure 4a) revealed two overlapping Gaussian-like distributions, the lower one associated with $\alpha_s$ lamellae and the higher one with $\alpha_p$ particles. The histogram for vanadium revealed two even more distinct Gaussian-like distributions with the lower one corresponding to $\alpha_p$ particles and the higher one

with $\alpha_s$ lamellae (Figure 4b). For this reason, the local minimum at which the two Gaussian-like histograms for *vanadium* intersected was chosen as the point separating $\alpha_p$ and $\alpha_s$ for binning EDS, inverse-pole-figure, pole-figure, and image-quality data. In other words, any datum with a vanadium concentration lower or higher than that corresponding to the point of intersection was considered to be $\alpha_p$ or $\alpha_s$, respectively (Figure 4c). *Manual* separation of the EBSD data (based on the shape of primary alpha particles) gave results similar to those obtained by partitioning the data automatically using the vanadium concentration. Furthermore, automatic separation of the EBSD data based on the *aluminum* concentration yielded similar results to those obtained by partitioning the data using the vanadium concentration. Additional support for the technique was obtained from measurements of the volume fraction of $\alpha_p$. Values of ~57 and ~61 pct. were obtained using automated partitioning of IPF data (Figure 4c) and quantitative metallography on BSE images, respectively.

### 4.3 Separation of $\alpha_p$ and $\alpha_s$ textures in hot-rolled Ti-6Al-4V

Using the partitioning of vanadium to bin points corresponding to $\alpha_p$ or $\alpha_s$, discrete (0001) pole figures for primary and secondary alpha were determined for the hot-rolled Ti-6Al-4V sample (Figure 5). The texture of the sample taken as a whole (i.e., the texture of $\alpha_p + \alpha_s$) showed three major texture components (Figure 5a): a strong one along the rolling direction (RD) of the plate, a second weaker one along the transverse direction (TD) of the plate, and the weakest one consisting of four spots lying at approximately 45° to the RD and TD. A comparison of the separated (0001) pole figures (Figure 5b, c) revealed that the TD and the 45° texture components were associated with the $\alpha_s$ phase (Figure 5c). In addition, both the $\alpha_s$ and $\alpha_p$ phases had a relatively strong texture component along the RD direction.

Insight into the nature of texture formation in the rolled plate was obtained from the microstructure of a specimen of the *unrolled* Ti-6Al-4V material that was heat treated at the rolling temperature (955°C) and then water quenched. The BSE micrograph of the *unrolled* Ti-6Al-4V material (Figure 6) indicated that only ~30 pct. of the microstructure was $\alpha_p$ at the rolling temperature. Due to the small amount of $\alpha_p$ at 955°C, the majority of the strain imposed during the rolling process at 955°C was thus most likely accommodated by the beta phase [11]. Hence, only small changes in the $\alpha_p$ texture relative to that in the undeformed material would be expected due to deformation. On the other hand, the $\alpha_s$ texture formed as a result of decomposition of heavily-worked beta. The aspects are discussed in the following sections.

### 4.4 Interpretation of beta-phase texture in hot-rolled Ti-6Al-4V

XRD measurements for the beta phase retained at room temperature in the hot-rolled Ti-6Al-4V plate (Figure 7) revealed a moderate texture. The ODF consisted of a ($45^o$, $0^o$, $0^o$) component and a {111} <uvw> fiber (so-called $\gamma$ fiber in rolled bcc metals) [2]. The current measurements are in good agreement with previous observations for hot rolled Ti-6Al-4V [12]. As mentioned in Section 4.3, a moderate-to-strong deformation texture might have been expected in the beta phase because it accommodates most of the imposed deformation during rolling at 955°C. The decomposition of beta to form $\alpha_s$ (plus a small amount of retained beta) typically follows the Burger relationship ($(0001)_\alpha$ parallel to $(101)_\beta$ [13]. As a result, the (0001) $\alpha_s$ and $(101)_\beta$ pole figures would be expected to be similar, as was indeed observed (i.e., Figures 5c and 7). The similar locations of the different texture components in these pole figures provided support for the usefulness of the EBSD/EDS technique. However, there were some

noticeable differences in the *intensity* of different components. The XRD $(101)_\beta$ pole figure showed high intensities at the 45° location as well as at the RD and TD locations. By contrast, the $\alpha_s$ (0001) pole figure showed the highest intensity at the TD direction and the lowest at 45°. Such differences are most likely related to preferential variant selection during the decomposition of the beta phase [12].

### 4.5 Comparison of EBSD/EDS and XRD methods

Results from the EBSD/EDS method for separating the textures of primary and secondary alpha in the hot-rolled Ti-6Al-4V plate were compared with those obtained using the XRD method of Glavicic, *et al.* [6]. The overall texture of the α phase ($\alpha_p+\alpha_s$) was determined via XRD from the same sample used for the EBSD/EDS technique. The (0001) pole figure for this sample (Figure 8a) showed the same three components as in the EBSD/EDS measurement. However, the magnitude of the XRD TD component was greater than that of the RD component, in contrast to the findings from the EBSD/EDS measurement (Figure 5a). Furthermore, the texture of the rolled sample heat treated at 955°C and furnace cooled to obtain a microstructure of equiaxed alpha (Figure 8b) exhibited a very strong RD component (~2.5 times as strong as the EBSD/EDS measurement) as well as very weak TD and 45° components which had been absent in the EBSD/EDS case. By subtracting the measured XRD $\alpha_p$ texture (weighted by its volume fraction in the rolled sample) from the XRD $\alpha_p+\alpha_s$ measurement, an estimate of the $\alpha_s$ texture was obtained (Figure 8c). The XRD (0001) pole figure so determined showed moderate TD and 45° components as did the EBSD/EDS sample, but lacked the RD component.

Several sources of the difference in the EBSD/EDS and XRD textures can be postulated. These factors include the overlap of the beta- and alpha-phase peaks in XRD data and the possible growth of different $\alpha_p$ components during the heat treatment process used in the Glavicic, *et al.* method to obtain the $\alpha_p$ texture. With regard to the first possibility, the (110) pole figure of the beta phase may be expected to be superimposed on and thus "contaminate" (0001) pole-figure data for the alpha phase in Ti-6Al-4V (for $\alpha_p+\alpha_s$ as well as $\alpha_p$) due to the proximity of the $(110)_\beta$ and $(0001)_\alpha$ diffraction peaks [14, 15]. This contamination may be the source of the TD and 45° components in the XRD $\alpha_p$ (0001) pole figure, which are not found in the EBSD/EDS measurement. From a quantitative standpoint, however, the degree of contamination depends on the volume fraction and relative strength of the texture of beta retained in Ti-6Al-4V at room temperature (~6 pct.).

The high intensity along the TD in the XRD $\alpha_p$ pole figure compared to that for the EBSD/EDS pole figure may be due to the preferential growth of a weak $\alpha_p$ texture component along the TD during furnace cooling to produce a fully-equiaxed alpha microstructure. Evidence for such an effect is presented in the following section.

### 4.6 Effect of slow cooling on preferential growth of primary alpha

The major assumption of the XRD method to separate the $\alpha_p$ and $\alpha_s$ textures [5] is that the $\alpha_p$ texture is preserved during high temperature solution treatment of the $\alpha_s$ and subsequent slow cooling that gives rise to epitaxial growth of the $\alpha_p$. However, observed differences between the room-temperature $\alpha_p$ texture of the hot-rolled Ti-6Al-4V determined by EBSD (Figure 5b) and that measured by XRD on a sample slow cooled following solution treatment (Figure 8b) cast doubt on this assumption.

The microstructure and texture of *unrolled* Ti-6Al-4V program material after a 4-hour heat treatment 955°C followed by either water quenching or furnace cooling to room temperature provided needed insight into this assumption and the possible growth of weak $\alpha_p$ texture components during slow cooling from high-temperature solution treatment. The microstructure of the water quenched (WQ) sample, for example, revealed 30 pct. $\alpha_p$ particles (dark) surrounded by martensite (Figure 9a). On the other hand, the furnace-cooled (FC) sample revealed 93 pct. $\alpha_p$ particles in a matrix of retained beta (Figure 9b).

The EBSD technique was used to determine the $\alpha_p$ texture of the unrolled FC sample. However, an alternate EBSD binning technique using image-quality (IQ) maps was found to be necessary for the unrolled WQ sample which contained a large volume fraction (~70 pct.) of martensite. The high dislocation density in martensitic alpha results in a very low IQ during the indexing of EBSD Kikutchi patterns. For the WQ sample, an OIM® IQ threshold of 200 was found to provide an accurate separation of data for the primary and martensitic alpha. Such a threshold yielded volume fractions of the phases in excellent agreement with quantitative metallography (using SEM BSE images) and an $\alpha_p$ texture identical to that derived by the tedious, manual-separation technique.

The $\alpha_p$ textures of the unrolled WQ and FC samples measured by EBSD over areas as large as 1.2 mm x 1.2 mm and in 10 different randomly-chosen areas revealed distinctive differences (Figure 10). Specifically, the WQ sample (Figure 10a) had only one texture component comprising basal poles along the RD. This $\alpha_p$ texture is thus similar to that *after* rolling at 955°C (Figure 5b) and supports the hypothesis that the primary alpha underwent relatively little strain during hot rolling high in the alpha/beta phase field. By contrast, the unrolled FC sample (Figure 10b) had two *additional* texture components, one along the TD with intensity greater than ~ 9 x random and components at 45° to the RD and TD with an intensity as high as 4 x random. These results thus strongly suggest that furnace cooling of the Ti-6Al-4V program material from a high solution temperature resulted in preferential growth of certain $\alpha_p$ components which were initially very weak.

The effect of water quenching versus furnace cooling on the $\alpha_p$ texture was further elucidated by measuring the texture over the *entire* sample surface by both EBSD and XRD. In particular, the $\alpha_p$ texture measured by EBSD for an area measuring 20 mm x 4.8 mm revealed similar and distinctive differences between the WQ and the FC samples (Figure 11) as in the smaller-area scans. Specifically, the basal texture along the TD was very weak for the WQ sample (~3 x random), but much stronger for the FC sample (~ 13 times random). On the other hand, the WQ sample had a higher-intensity basal texture along the RD (~13 x random) in comparison to that for the FC sample (< 9 times random).

Further examination of the EBSD results revealed that the texture component at 45° to the RD and TD was much weaker in large-area (20 mm x 4.8 mm) scans (Figure 11) compared to smaller-area (1.2 mm x 1.2 mm) scans (Figure 10). This difference can be explained by microtexture found in the unrolled WQ and FC samples, as illustrated by. RD IPF maps (Figures 12 and 13). The microtexture was more pronounced in the FC sample (Figure 12b and 13b), lending credence to the hypothesis that furnace cooling results in preferential growth of certain $\alpha_p$ texture components.

XRD gave similar results for the $\alpha_p$ texture of the FC sample. However, XRD determination of the $\alpha_p$ texture for the WQ sample was not possible because of the presence of the large volume fraction (~ 70 pct.) of martensitic alpha whose diffraction peaks overlap those of the $\alpha_p$ phase.

Several sources of preferential growth of the primary-alpha particles can be hypothesized. First, if the TD/45° textures are associated with globular particles which are *smaller* than those containing the RD texture, faster diffusional growth of the former during furnace cooling would be expected [9]. Second, a variation in morphology would affect the rates of growth of alpha particles during cooling. As discussed recently [16], the growth of remnant lamellar plates can be much slower than globular particles, the exact difference depending on the size of the particles and the thickness and the diameter-to-thickness ratio of the plates. Such differences in size or morphology of the primary alpha could easily be developed during breakdown rolling of a lamellar microstructure. Alpha plates whose c-axis is along the RD would be difficult to deform/spheroidize during rolling and thus tend to retain their morphology [17]. On the other hand, alpha plates whose c-axis is along the TD (or 45° to the RD and TD) would deform and spheroidize readily [17]. Such possibilities are now under investigation.

## 5.0 SUMMARY AND CONCLUSIONS

An EBSD/EDS method to separate the textures of primary alpha and secondary-alpha colonies in alpha-beta titanium alloys with a duplex microstructure was developed. This technique is based on binning each discrete EBSD measurement according to its chemical composition as determined by simultaneous EDS. The approach was applied to hot-rolled Ti-6Al-4V in which the partitioning of vanadium provides the most noticeable signature for automated discrimination of primary-alpha particles ($\alpha_p$) and the secondary-alpha colonies ($\alpha_s$), the latter formed by decomposition of beta phase during cooling. The results for this material showed the following:

1. The primary-alpha (deformation) texture is aligned with the rolling direction.
2. The secondary-alpha (transformation) texture was correlated (through the Burgers relation between beta and alpha) to the deformation texture of the beta phase with principal components along the TD and at ~ 45° to the RD and TD.
3. Quantitative differences in the intensity of specific components in the $\alpha_s$ and parent beta textures suggested preferential variant selection during the transformation.
4. Furnace cooling from 955°C may cause preferential growth of weak primary-alpha texture components and lead to noticeable microtexture.
6. For water-quenched samples containing a large volume fraction of martensitic alpha, a binning technique similar to EBSD/EDS, but based on image quality, can be used for automated texture separation.

## 6.0 REFERENCES


1. G. Lutjering, *Materials Science and Engineering A* A243 (1998) 32-45.
2. U.F. Kocks, C.N. Tome, H.R. Wenk, *Texture and Anisotropy*, Cambridge University Press, Cambridge, United Kingdom, 1998, pp. 129-176.
3. L. Germain, N. Gey, M. Humbert, A. Hazotte, P. Bocher, M. Jahazi, *Materials Characterization* 54 (2005) 216-222.
4. L. Germain, N. Gey, P. Bocher, M. Jahazi, *Material Science Forum* 495-497 (2005) 663-668.
5. M.J. Thomas, B.P. Wynne, W.M. Rainforth, *Materials Characterization* 55 (2005) 388-394.
6. M.G. Glavicic, J.D. Miller, S.L. Semiatin, *Scripta Materialia* 54 (2006) 281-286.
7. EDAX, Inc., 392 East 12300 South, Suite H., Draper, UT 84020.
8. Los Alamos Polycrystal Plasticity Code, Los Alamos National Laboratory, Report LA-CC-88-6, 1988.
9. S.L. Semiatin, S.L. Knisley, P.N. Fagin, F. Zhang, D.R. Barker, *Metall. Mater. Trans. A* 34A (2003) 2377-2386.
10. R. Castro, L. Seraphin, *Mém. Sci. Rev. Metall.* 63 (1966) 1025-1058.
11. S.L. Semiatin, F. Montheillet, G. Shen, J.J. Jonas, *Metall. Mater. Trans. A* 33A (2002) 2719-2727.
12. N. Gey, M. Humbert, M.J. Philippe, Y. Combres, *Materials Science and Engineering A* A230 (1997) 68-74.
13. W.G. Burgers, *Physica* 1 (1934) 561-586.
14. M.G. Glavicic and S.L. Semiatin, *Acta Materialia* 54 (2006) 5337-5347.
15. S.L. Semiatin, P.N. Fagin, M.G. Glavicic, I.M. Sukonnik, and O.M. Ivasishin, *Materials Science and Engineering A* A299 (2001) 225-234.
16. S.L. Semiatin, T.M. Lehner, J.D. Miller, R.D. Doherty, D.U. Furrer, *Metall. Mater. Trans. A*, 38A (2007) in press.
17. T.R. Bieler, S.L. Semiatin, *Inter. J. Plasticity*, 18 (2002) 1165-1189.

**Figure Captions**

Figure 1 Ti-6Al-4V microstructures: (a) SEM secondary-electron image for material with a duplex microstructure of globular $\alpha_p$ and colonies of $\alpha_s$, (b) low magnification backscattered-electron (BSE) image revealing $\alpha_p$ particles as dark areas and $\alpha_s$ colonies as light gray areas, (c) high magnification BSE image revealing the similarity in darkness of both $\alpha_p$ particles and thick $\alpha_s$ in lamellar colonies, and (d) optical micrograph of an electropolished-and-etched surface revealing $\alpha_p$ particles and $\alpha_s$ colonies.

Figure 2 SEM BSE images of hot-rolled Ti-6Al-4V: (a) as-deformed, and (b) after epitaxial growth of the $\alpha_p$ particles via furnace cooling from the solution temperature.

Figure 3 SEM results for an electropolished sample of hot-rolled Ti-6Al-4V: (a) secondary-electron image, (b) normal-direction inverse-pole-figure map revealing $\alpha_p$ and $\alpha_s$ regions which are not distinguishable, (c) image-quality map of the same area as (b) with no clear difference between $\alpha_s$ and $\alpha_p$, (d) EDS map for aluminum, and (e) EDS map for vanadium. In the EDS maps (d, e), dark or light shading is associated with a lower or a higher concentration, respectively, of the particular alloying element.

Figure 4 EDS results for hot-rolled Ti-6Al-4V: (a) aluminum histogram, (b) vanadium histogram with $\alpha_s$ in light gray, and (c) the corresponding microstructure partitioned based on vanadium content. In (c), $\alpha_s$ colonies are light gray.

Figure 5 Alpha-phase (0001) pole figures for hot-rolled Ti-6Al-4V determined by the EBSD/EDS technique and vanadium partitioning: (a) $\alpha_p + \alpha_s$ texture, (b) $\alpha_p$ particles, and (b) $\alpha_s$ colonies.

Figure 6 Backscattered-electron image of the microstructure developed in undeformed Ti-6Al-4V during solution treatment at the rolling temperature (955°C) followed by water quenching.

Figure 7 Beta-phase (110) pole figure for hot-rolled Ti-6Al-4V determined by XRD.

Figure 8 Alpha-phase (0001) pole figures for hot-rolled Ti-6Al-4V determined using the XRD technique of Glavicic, *et al.* [6]: (a) measured $\alpha_p + \alpha_s$ texture, (b) measured $\alpha_p$ texture, and (b) calculated $\alpha_s$ texture.

Figure 9 SEM BSE images of the microstructure developed in the *unrolled* Ti-6Al-4V program material during heat treatment at 955°C for 4 hours followed by (a) water quenching or (b) furnace cooling.

Figure 10 Alpha-phase (0001) pole figures determined by EBSD for *unrolled* Ti-6Al-4V heat treated 4 hours at 955°C followed by (a) water quenching or (b) furnace cooling. Scanned areas were 1.2 mm x 1.2 mm.

Figure 11 Alpha-phase (0001) pole figures determined by EBSD for *unrolled* Ti-6Al-4V heat treated 4 hours at 955°C followed by (a) water quenching or (b) furnace cooling. Scanned areas were 20 mm x 4.8 mm.

Figure 12 Rolling-direction IPF maps determined by EBSD for *unrolled* Ti-6Al-4V heat treated 4 hours at 955°C followed by (a) water quenching or (b) furnace cooling. Scanned areas were 1.2 mm x1.2 mm. The rolling direction is horizontal.

Figure 13 Rolling-direction IPF maps determined by EBSD for *unrolled* Ti-6Al-4V heat treated 4 hours at 955°C followed by (a) water quenching or (b) furnace cooling. Scanned areas were 20 mm x 4.8 mm. The c-axis was primarily aligned close to the RD in the red areas and close to the TD in the blue areas. The rolling direction is horizontal.

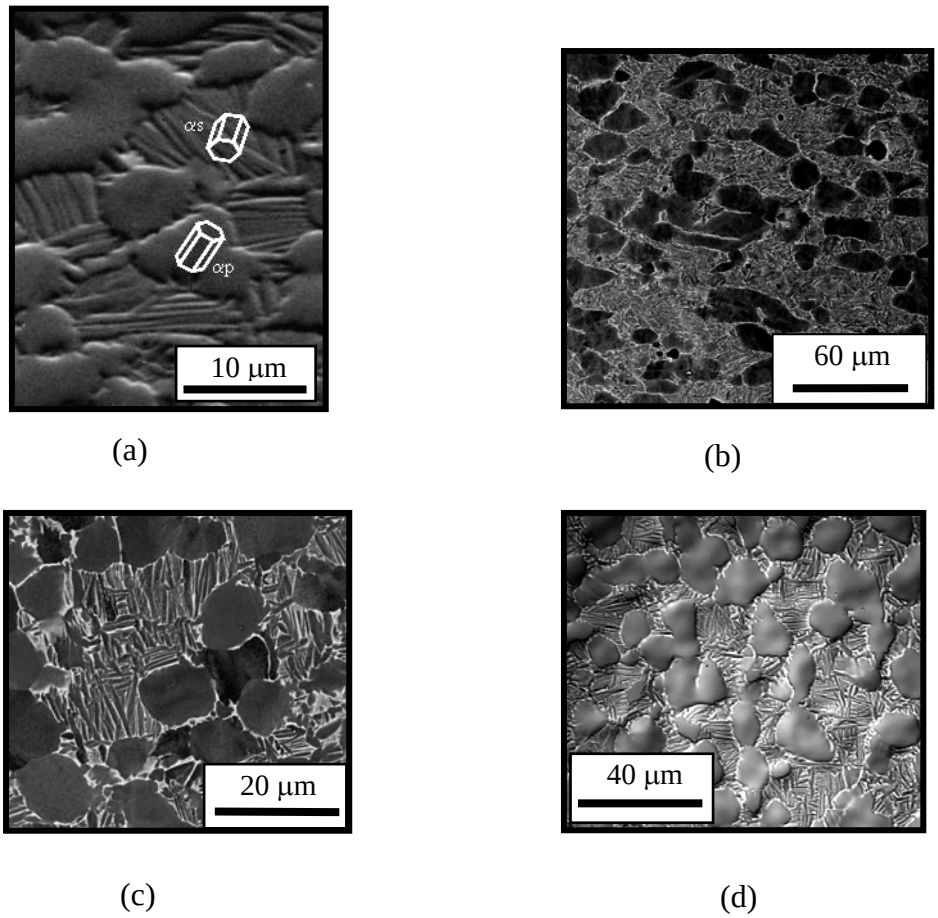


Figure 1. Ti-6Al-4V microstructures: (a) SEM secondary-electron image for material with a duplex microstructure of globular $\alpha_p$ and colonies of $\alpha_s$, (b) low magnification backscattered-electron (BSE) image revealing $\alpha_p$ particles as dark areas and $\alpha_s$ colonies as light gray areas, (c) high magnification BSE image revealing the similarity in darkness of both $\alpha_p$ particles and thick $\alpha_s$ in lamellar colonies, and (d) optical micrograph of an electropolished-and-etched surface revealing $\alpha_p$ particles and $\alpha_s$ colonies.

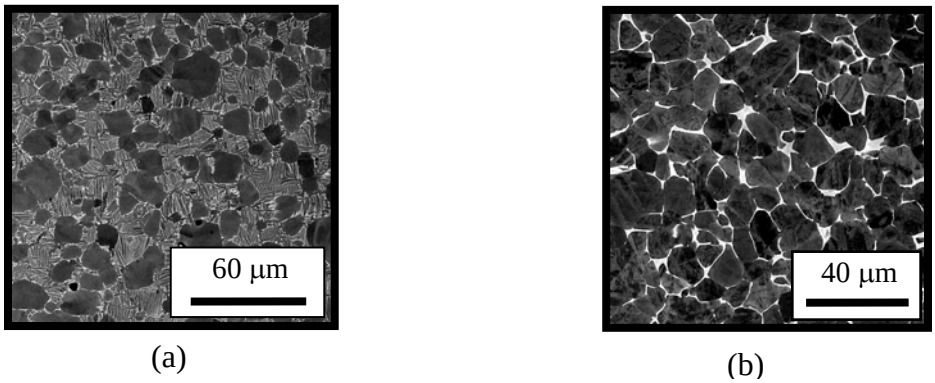


Figure 2. SEM BSE images of hot-rolled Ti-6Al-4V: (a) as-deformed, and (b) after epitaxial growth of the $\alpha_p$ particles via furnace cooling from the solution temperature.

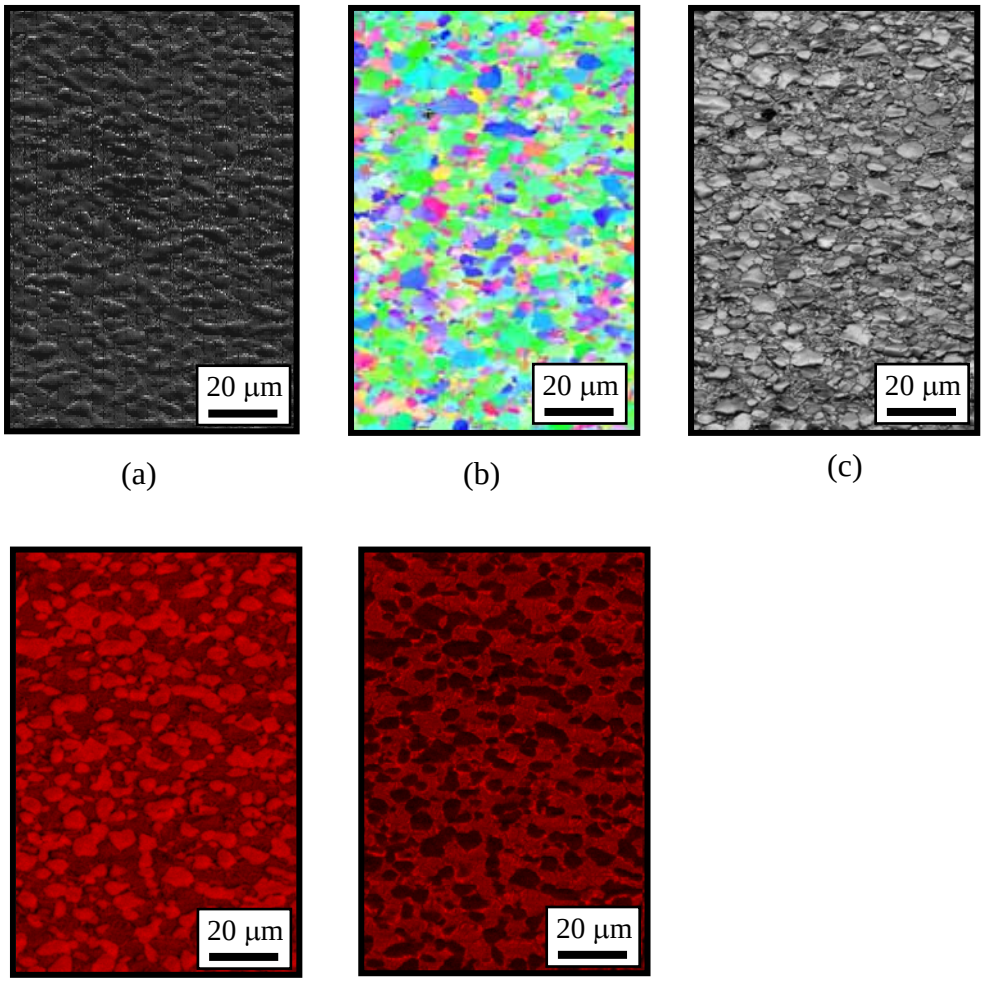


Figure 3. SEM results for an electropolished sample of hot-rolled Ti-6Al-4V: (a) secondary-electron image, (b) normal-direction inverse-pole-figure map revealing $\alpha_p$ and $\alpha_s$ regions which are not distinguishable, (c) image-quality map of the same area as (b) with no clear difference between $\alpha_s$ and $\alpha_p$, (d) EDS map for aluminum, and (e) EDS map for vanadium. In the EDS maps (d, e), dark or light shading is associated with a lower or a higher concentration, respectively, of the particular alloying element.

.

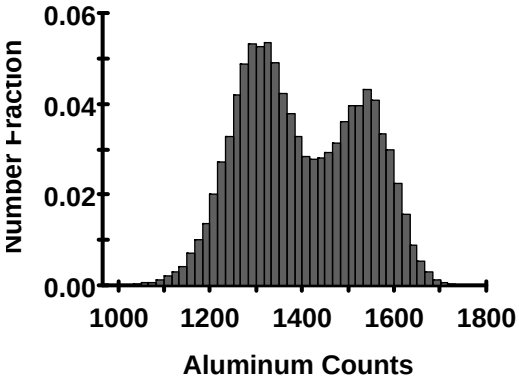


(a)

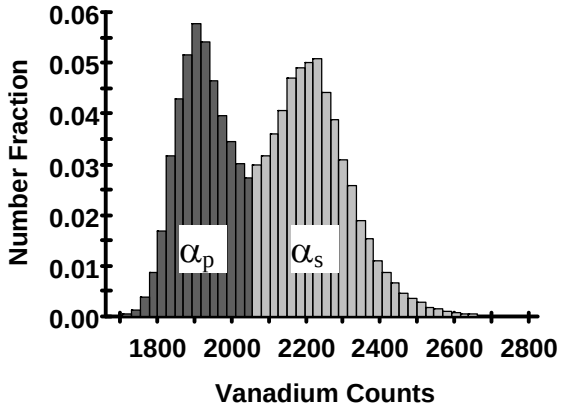


(b)


(c)

Figure 4. EDS results for hot-rolled Ti-6Al-4V: (a) aluminum histogram, (b) vanadium histogram with $\alpha_s$ in light gray, and (c) the corresponding microstructure partitioned based on vanadium content. In (c), $\alpha_s$ colonies are light gray.

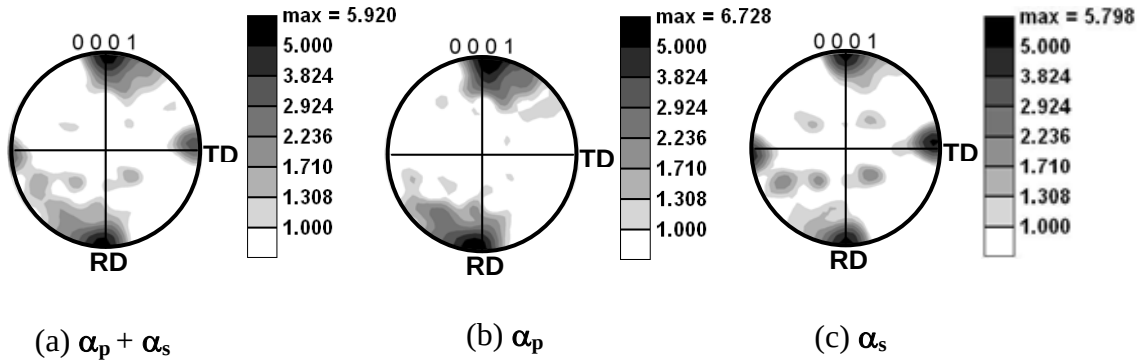


(a) $\alpha_p + \alpha_s$ (b) $\alpha_p$ (c) $\alpha_s$

Figure 5. Alpha-phase (0001) pole figures for hot-rolled Ti-6Al-4V determined by the EBSD/EDS technique and vanadium partitioning: (a) $\alpha_p + \alpha_s$ texture, (b) $\alpha_p$ particles, and (b) $\alpha_s$ colonies.

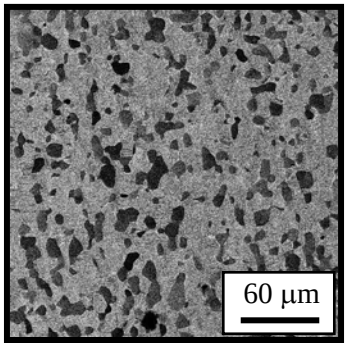


Figure 6. Backscattered-electron image of the microstructure developed in undeformed Ti-6Al-4V during solution treatment at the rolling temperature (955°C) followed by water quenching.

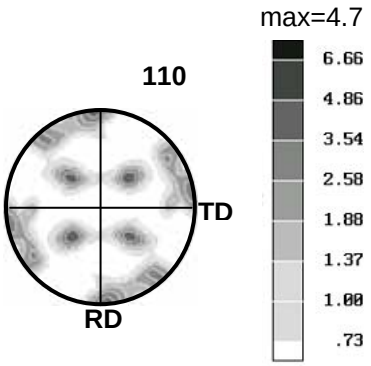


Figure 7. Beta-phase (110) pole figure for hot-rolled Ti-6Al-4V determined by XRD.

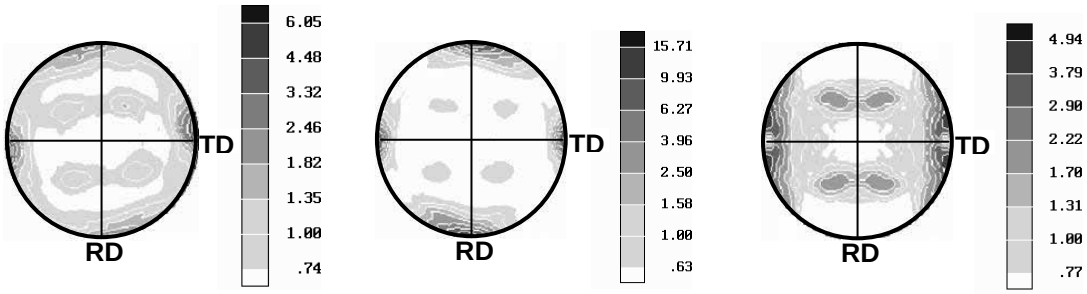


(a) $\alpha_p + \alpha_s$ (b) $\alpha_p$ (c) $\alpha_s$

Figure 8. Alpha-phase (0001) pole figures for hot-rolled Ti-6Al-4V determined using the XRD technique of Glavicic, *et al.* [6]: (a) measured $\alpha_p + \alpha_s$ texture, (b) measured $\alpha_p$ texture, and (b) calculated $\alpha_s$ texture.

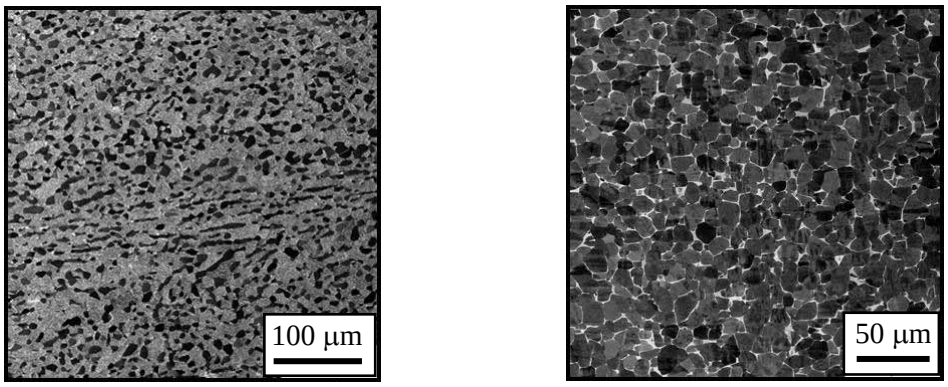


(a) (b)

Figure 9. SEM BSE images of the microstructure developed in the *unrolled* Ti-6Al-4V program material during heat treatment at 955°C for 4 hours followed by (a) water quenching or (b) furnace cooling.

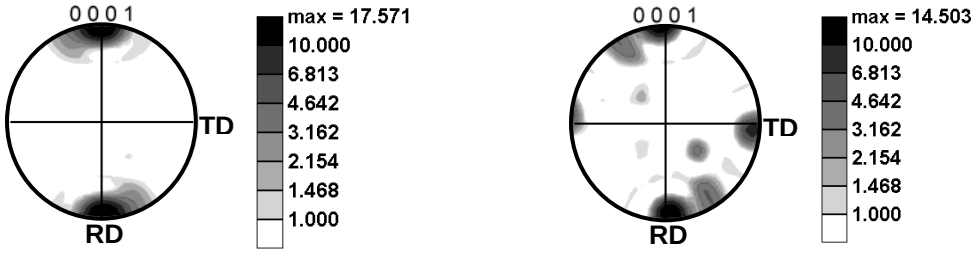


(a) (b)

Figure 10. Alpha-phase (0001) pole figures determined by EBSD for *unrolled* Ti-6Al-4V heat treated 4 hours at 955°C followed by (a) water quenching or (b) furnace cooling. Scanned areas were 1.2 mm x 1.2 mm.

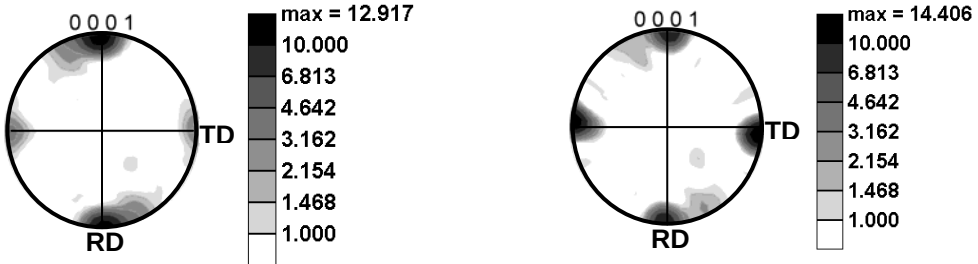


(a) (b)

Figure 11. Alpha-phase (0001) pole figures determined by EBSD for *unrolled* Ti-6Al-4V heat treated 4 hours at 955°C followed by (a) water quenching or (b) furnace cooling. Scanned areas were 20 mm x 4.8 mm.

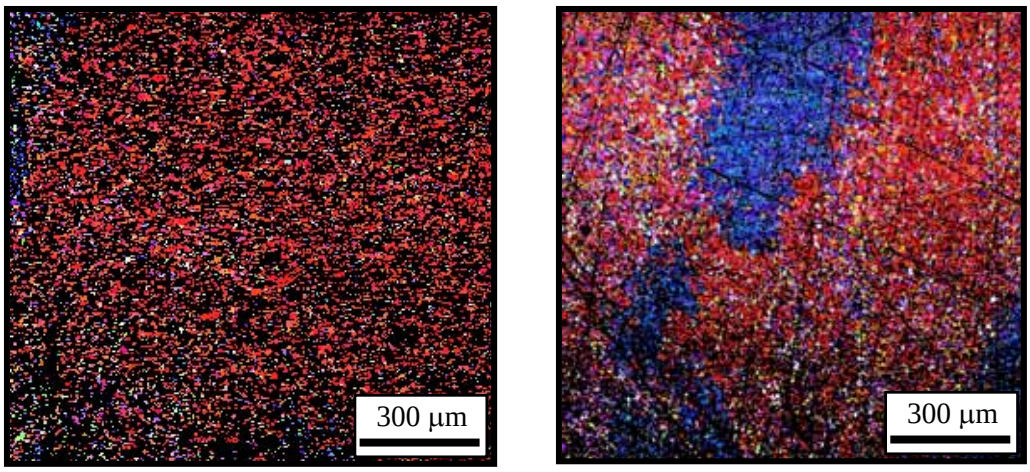


(a) (b)

Figure 12. Rolling-direction IPF maps determined by EBSD for *unrolled* Ti-6Al-4V heat treated 4 hours at 955°C followed by (a) water quenching or (b) furnace cooling. Scanned areas were 1.2 mm x1.2 mm. The rolling direction is horizontal.

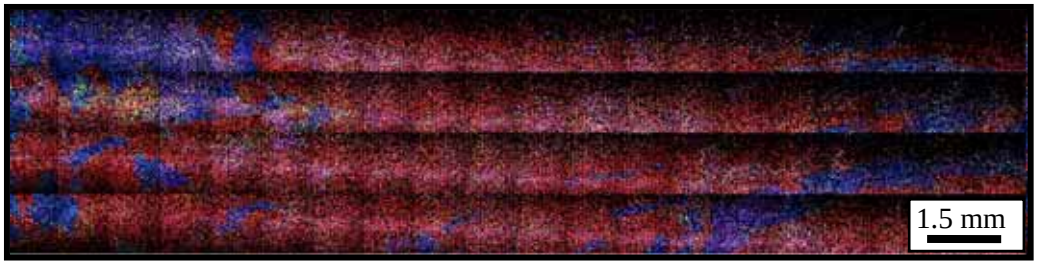


(a)

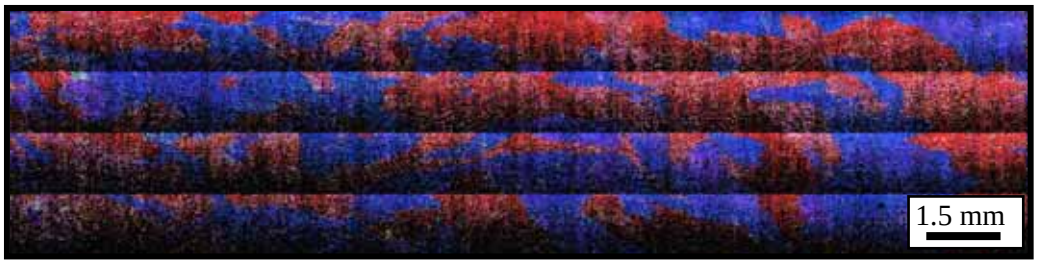


(b)

Figure 13. Rolling-direction IPF maps determined by EBSD for *unrolled* Ti-6Al-4V heat treated 4 hours at 955°C followed by (a) water quenching or (b) furnace cooling. Scanned areas were 20 mm x 4.8 mm. The c-axis was primarily aligned close to the RD in the red areas and close to the TD in the blue areas. The rolling direction is horizontal.

# The Effect of Preheat Temperature and Inter-Pass Reheating on Microstructure and Texture Evolution during Hot Rolling of Ti-6Al-4V

A.A. Salem[a*], M.G. Glavicic[b], and S.L. Semiatin
Air Force Research Laboratory, Materials and Manufacturing Directorate,
AFRL/RXLM, Wright-Patterson AFB, OH 45433
[a] Universal Technology Corp., 1270 N. Fairfield Road, Dayton, OH 45432
[b] UES Inc., 4401 Dayton-Xenia Road, Dayton, OH 45433

## Abstract

The effect of preheat temperature and inter-pass reheating on microstructure and texture evolution during unidirectional hot rolling of Ti-6Al-4V in the alpha + beta field was investigated. Three different heating schedules were used to roll plates at 10 pct. reduction per pass to a 3:1 total reduction (true strain = 1.15): (1) preheat at 955°C with inter-pass reheating for 3 minutes, (2) preheat at 955°C without inter-pass reheating, and (3) preheat at 815°C with inter-pass reheating for 3 minutes. Following rolling, each plate was air cooled to simulate production practice. The microstructures and textures were determined using electron-backscatter and X-ray diffraction techniques. The results revealed that the intensity of basal poles decreased along the rolling direction and increased along the normal and transverse directions with decreasing rolling (furnace) temperature or the elimination of reheating between passes.

*Keywords:* Ti-6Al-4V alloy, hot rolling, texture, reheating

## Acknowledgements

This work was conducted as part of the in-house research activities of the Metals Processing Group of the Air Force Research Laboratory's Materials and Manufacturing Directorate. The support and encouragement of the Laboratory management and the Air Force Office of Scientific Research (Dr. J. Fuller, program manager) are gratefully acknowledged. The assistance of R. Wheeler in conducting the experimental work is much appreciated. Two of the authors were supported through Air Force Contracts F33615-03-D-5801 (AAS) and FA8650-04-D-5235 (MGG).

* Corresponding author (e-mail: ayman.salem@wpafb.af.mil)

## 1.0 INTRODUCTION

Alpha/beta titanium alloys provide an excellent combination of high strength, corrosion resistance, and low density. Hence, they are widely used for many applications, especially in the aerospace industry. Accounting for approximately 80 pct. of the total usage in the US market [1], Ti-6Al-4V is the most common material in this class. The mechanical behavior of the material can be tailored by altering microstructure and texture through judicious choice of thermomechanical processing (TMP) parameters [2-4].

In general, three broad types of microstructures can be developed in alpha/beta titanium alloys by TMP [2-4], namely, fully lamellar, fully equiaxed, and duplex (bi-modal). A mixture of equiaxed particles of primary alpha ($\alpha_p$) and lamellae of secondary alpha ($\alpha_s$) in a matrix of beta ($\beta$) phase comprises the duplex microstructure. Numerous applications require the duplex microstructure due to its good yield strength and ductility, fatigue-crack-initiation resistance, and slow fatigue-crack-propagation rate [5].

The duplex microstructure can exhibit moderate-to-strong crystallographic textures that develop during large deformation in the alpha + beta phase field. For example, unidirectional rolling usually gives rise to two major types of textures: the so-called basal/transverse (B/T), in which the alpha-phase basal poles are located along the plate-normal and long-transverse directions, and transverse (T) [3, 4]. Low temperature deformation tends to result in the B/T texture while high temperature deformation (close to the beta transus at which alpha + beta $\rightarrow$ alpha) results in the T texture.

Previous research for titanium alloys with a duplex microstructure has focused for the most part on the overall texture of the alpha phase, without separating that of the $\alpha_p$ and $\alpha_s$ micro-constituents. However, the textures of $\alpha_p$ and $\alpha_s$ evolve primarily as a result of either the deformation in the two-phase field or the decomposition of the hot-worked beta matrix during cooling, respectively. Thus $\alpha_p$ and $\alpha_s$ may be expected to develop different texture components during TMP.

The separation of the $\alpha_p$ deformation texture and the $\alpha_s$ transformation texture is complicated by the fact that the alpha phase in each instance consists of the same crystal structure and lattice parameters. Consequently, it is very difficult to distinguish between them using standard measurements techniques based on x-ray or electron-backscatter diffraction (XRD, EBSD) [6, 7]. Because the morphology and texture of $\alpha_p$ particles and $\alpha_s$ lamellae each have a major influence on final mechanical properties, a number of techniques are now under development to meet this need [6, 7].

The current work was undertaken as part of a larger program to apply advanced characterization techniques to quantify the effect of TMP parameters on the evolution of microstructure and texture in alpha/beta titanium alloys such as Ti-6Al-4V. The specific objective of the present effort was to establish the effect of rolling temperature and reheat schedule on microstructure and texture development. For this purpose, techniques based on simultaneous EBSD and EDS (electron-dispersive spectroscopy) or EBSD image-quality maps were used to separate the textures of primary and secondary alpha [6].

## 2.0 MATERIAL AND EXPERIMENTAL PROCEDURES

### 2.1 Material

The material used in the present program was identical to that employed previously [6]. It comprised Ti-6Al-4V which was received as 32-mm-thick plate having a measured composition (in weight pct.) of 6.15 aluminum, 3.9 vanadium, 0.20 oxygen, 0.21 iron, 0.008 nitrogen, 0.01 carbon, 0.0031 hydrogen, and balance titanium. The beta transus temperature was 995 °C [8].

The as-received Ti-6Al-4V material was heated to 955°C, thus dissolving all $\alpha_s$ lamellae from prior processing, soaked for four hours, and furnace cooled to produce a microstructure of ~95 pct. equiaxed-alpha particles ($\alpha_p$) in a matrix of retained beta. Selected samples were water quenched from 955°C in order to quantify the texture (and microstructure) of the primary alpha present at the soak temperature.

### 2.2 Experimental procedures

The broad effect of TMP parameters on microstructure and texture development was determined by conventional hot rolling of samples measuring 32 x 38 x 76 mm that were cut from the heat-treated-and-furnace-cooled material. The preform width (38 mm) was limited by the load capacity of the two-high rolling mill that was used. Each preform was furnace heated to a temperature of either 815 or 955°C, soaked for 40 minutes, and hot rolled at a speed of 30 m/min to a 3:1 total reduction using a 10-pct. reduction per pass and a reheat time between passes of three minutes. To provide further insight into the effect of heating schedule on texture and microstructure development, an additional perform was rolled in a similar fashion using a furnace (preheat) temperature 955°C but without inter-pass reheating. The majority of the samples were rolled parallel to the original rolling direction of the as-received plate; selected samples were rolled perpendicular to the original rolling direction. Each of the samples was air cooled following rolling to mimic industrial practice.

To characterize microstructure and texture, samples of the unrolled material and the hot-rolled plates were sectioned along the mid-plane, ground, and electropolished at -20°C in a solution of 590 ml methanol and 60 ml perchloric acid. Following electropolishing, each sample was mounted on the tilting stage inside an XL30 field-emission-gun scanning-electron-microscope (FEG-SEM). The microscope was operated at 20 kV and 7 nA with the stage tilted at an inclination of 70°.

Kikuchi patterns were collected using an EBSD system from EDAX [9]. In addition, the local composition was determined via simultaneous EDS analysis. A 0.3-μm step size was used to cover an area measuring 80 μm x 120 μm. Different step sizes and larger areas (within the maximum of 25 mm x 25 mm associated with the microscope construction) were also utilized. The textures of $\alpha_p$ and $\alpha_s$ were separated using the EBSD/EDS technique described in Ref. 6.

The texture results from the present technique were compared to those obtained using the x-ray-diffraction (XRD) approach developed previously by Glavicic, *et al.* [7]. For this purpose, an additional sample was removed from each of the hot-rolled Ti-6Al-4V plates. Each of these pieces was then cut into two equal sections. One half was analyzed in the as-hot-rolled condition. The other was given a one-hour heat treatment just above the rolling temperature followed by furnace cooling to produce an alpha microstructure that was fully globular; i.e.,

samples rolled at 950°C were annealed at 960°C while the sample rolled at 815°C was annealed at 820°C. The volume fraction of primary alpha in the as-hot-rolled duplex microstructure was determined by analysis of backscattered electron (BSE) images taken in a Leica-Cambridge Stereoscan 360 FEG-SEM. Subsequently, both pieces were prepared for XRD on the RD-TD plane at the mid-thickness of the rolled plate using standard metallographic techniques. XRD measurements were conducted using Cu Kα radiation from an 18 kW rotating anode source, and textures were determined from measurements of partial (10**Error! Objects cannot be created from editing field codes.**0), (0002), (10**Error! Objects cannot be created from editing field codes.**1), (10**Error! Objects cannot be created from editing field codes.**1), and (11**Error! Objects cannot be created from editing field codes.**0) alpha-phase pole figures. In addition, partial (110) and (200) beta-phase pole figures were determined to enable a comparison of the $\alpha_s$ texture and the texture of the parent beta phase. The partial pole figures were completed using the orientation-distribution-function (ODF) software in popLA (preferred orientation package from Los Alamos National Laboratory) [10].

## 3.0 RESULTS AND DISCUSSION

Microstructure and texture results demonstrated a marked dependence on rolling temperature primarily due to the associated variation in the volume fractions of the alpha and beta phases. The volume fraction of alpha is ~0.70 at 815°C and ~0.3 at 955°C [11]. These differences affect the relative partitioning of strain between the two phases [12] and thus the evolution of deformation texture as well as the development of the secondary-alpha texture due to decomposition of the hot-worked beta matrix.

### 3.1 Microstructure evolution

BSE micrographs revealed a noticeable dependence of microstructure on processing variables. The microstructure of the starting material heated 4 h at 955°C and water quenched (Figure 1a) contained 30 pct. $\alpha_p$ in a matrix of fine martensitic alpha in agreement with the results for Ti-6Al-4V in Reference 11. By contrast, furnace cooling following the heat treatment at 955°C produced ~93 pct. equiaxed alpha in a matrix of retained beta (Figure 1b). The absence of any transformation product in the furnace-cooled sample confirmed the appropriateness of the heat treatment to dissolve all secondary-alpha lamellae in the as-received material, and therefore assured that the measured secondary-alpha textures were due solely due to the prescribed TMP practices.

BSE micrographs of the hot-rolled materials (Figure 2) mirrored their respective processing parameters, denoted here as HTWR (rolled from a furnace at 955°C with inter-pass reheats), HTNR (rolled from a furnace at 955°C without inter-pass reheats), and LTWR (rolled from a furnace at 815°C with inter-pass reheats). Routes HTWR and HTNR both showed a duplex microstructure with a mixture of $\alpha_p$ and $\alpha_s$ lamellar colonies. High magnification BSE micrographs (Figures 2d, e) revealed shorter and more-highly deformed $\alpha_s$ platelets after HTNR compared to those developed during HTWR. In addition, the volume fractions of $\alpha_p$ were 0.61 and 0.45 for the HTWR and HTNR routes, respectively. The difference between the volume fraction of $\alpha_p$ in the HTWR sample compared to that in the sample water quenched from 955°C suggested that the cooling rate after the final pass was slow enough to enable some growth of the $\alpha_p$ prior to the decomposition of the beta matrix. Measurements of the surface temperature and rolling pressure at the completion of the HTNR sequence indicated that the temperature within this perform had dropped to ~815°C during transfer from the furnace and the various rolling passes prior to final air cooling. In this case, the lack of a large amount of growth of $\alpha_p$ may be ascribed to the rapid decomposition of the beta matrix due to concurrent deformation, thus providing a strong pinning tendency and reducing the supersaturation required for growth of $\alpha_p$.

Compared to the observations for samples rolled using a furnace temperature of 955°C, the microstructure for route LTWR did not show any signs of $\alpha_s$ lamellae (Figures 2c, f). The volume fraction of $\alpha_p$ in this sample (0.81) was comparable to that in material preheated at 815°C and water quenched, i.e., 0.70.

### 3.2 Texture evolution

Texture evolution during preheating and after the three different rolling processes was quantified using (0001) alpha-phase pole figures for $\alpha_p + \alpha_s$, for $\alpha_p$ by itself, and for $\alpha_s$ by itself. Selected beta-phase textures were also determined and represented using (110) pole figures.

### 3.2.1 Combined $\alpha_p + \alpha_s$ textures

The combined texture of the primary and secondary alpha ($\alpha_p+\alpha_s$) revealed a noticeable dependence on processing parameters. For the unrolled material, furnace cooling from 955°C produced a strong texture comprising basal poles along the rolling and transverse directions (RD and TD) with almost similar intensity. Water quenching led to a major texture component along the RD only (Figure 3). In both cases, the high intensities of different texture components resulted from microtexture in the as-received material [13].

The intensity and nature of the texture components was greatly reduced by rolling (Figure 4). Specifically, the times-random intensities were reduced from ~15 to ~5. Furthermore, the intensity along the TD was greater and the intensity along the RD was less for the lower rolling temperature (i.e., 815°C) with reheats (Figure 4c) compared to the intensities for the sample rolled at 955°C with reheats (Figures 4a). Moreover, a new component appeared with the c-axis titled ~20° from the ND towards the RD for the sample rolled at 815°C. Rolling from a 955°C furnace *without* reheating had a similar but weaker effect on the texture components compared to the observations for low-temperature rolling. That is to say, there was a measurably greater intensity of basal poles along the TD and a component with the c-axis titled from the ND towards the RD (Figure 4b).

The measured textures contrast somewhat with results in literature [2-4, 14], an effect that may be ascribed to differences in starting microstructure and texture as well as reheating practices. In particular, the work by and Peters and Luetjering [4] utilized Ti-6Al-4V with a random starting texture and a transformed beta microstructure; rolling was done with 2-min intermediate heating between passes. A B/T-type texture was obtained at low rolling temperatures at which a high volume fraction of alpha is present during deformation. At temperatures high in the alpha + beta phase field, at which the volume fraction of beta is large, a *beta* deformation texture was developed during rolling. To rationalize the T texture of the *alpha* phase formed during cooling from these temperatures, therefore, Peters and Luetjering concluded that preferential variant selection occurred during decomposition of the beta; i.e., during the cooling process, alpha phase formed on only one of the six possible {110} planes of the beta phase that satisfy the Burgers relationship $(0002)_\alpha \parallel (110)_\beta$.[15]. According to Frederick [16], the favored variant(s) are controlled by the strain imposed during the rolling process. For samples rolled at *intermediate* temperatures in the two-phase field, the intensity of the alpha-phase deformation texture (B/T) would tend to decrease because of partial alpha-phase accommodation of the imposed strain, and the T texture associated with beta transformation would be of low intensity due to the moderate volume fraction of beta present during deformation [16]. Consequently, a fairly weak overall alpha-phase texture is observed at intermediate rolling temperatures [4].

In contrast to the work of Peters and Luetjering [4], the *starting* texture was not random for the present material. It had basal poles along both the RD and TD. Because high temperature rolling tends to produce the T type texture, the intensity of the texture component along the TD in the present material would tend to predominate relative to the one along the RD for rolling at 955°C with reheats, as was observed (Figure 4a). Reheating between passes in the present work may have tended to lessen the tendency to form a sharp beta deformation texture (and the associated alpha texture developed during transformation) due to static recrystallization

and thus explain the low overall texture intensity formed during rolling at 955°C compared to that found by Peters and Luetjering [4].

Because deformation at low temperatures tends to yield a B/T type (deformation) texture, rolling at 815°C in the present work would tend to weaken the intensity of the basal poles along the RD and strength the ones along the TD, as was observed (Figure 4c). In addition, a component comprising basal poles along the normal direction (ND) would develop, in line with the appearance of the component titled ~20° from the ND.

Hot rolling from a furnace at 955°C without reheating between passes represents a scenario combining features of the other two sequences. During the initial passes, the T type texture would be dominant, while at the end of the rolling the development of the B/T type of texture would be promoted. The net result was a high intensity of basal poles along the TD and a weaker intensity of the B-type texture compared to rolling at 815°C with reheats (Figure 4c).

Cross rolling (i.e., rolling 90° to the reference/rolling direction in the starting material) led to textures which were similar to those in material rolled parallel to the reference direction (Figures 4d, e).

### 3.2.2 Primary-alpha ($\alpha_p$) textures

Separation of the primary-alpha ($\alpha_p$) texture from the overall alpha-phase texture using the EBSD/EDS and EBSD/image-quality techniques provided further insight into the effect of rolling temperature and reheating on texture formation.

For the sample rolled at 955°C with inter-pass reheating, for example, EBSD measurements revealed that a majority of the basal poles in the $\alpha_p$ texture were aligned with the RD (Figure 5a), in contrast to the slight predominance of the TD component for the overall texture (Figure 4a). Moreover, the $\alpha_p$ texture was seen to be stronger after separation from the weak overall texture developed during rolling at 955°C (Figure 4b). A masking effect of the $\alpha_p$ texture by the overall texture can be ascribed to the small volume fraction of primary alpha at 955°C. Furthermore, there was no evidence of texture components lying at 45° to the RD (i.e., $\gamma$ fiber) in the $\alpha_p$ texture following rolling at 955°C, in contrast to the observation for the unrolled-and-furnace-cooled material (Figure 3a).

Further examination of the texture of the unrolled material which was annealed at 955°C and then water quenched (Figure 3b) provided a plausible explanation for the strong $\alpha_p$ RD component following rolling at 955°C. Because of the poor image quality of the martensitic alpha, the pole figure in Figure 3b pertains to the *primary alpha* at 955°C. A comparison of Figures 3b and 5a thus reveals that the $\alpha_p$ texture after rolling at 955°C was largely inherited from the starting $\alpha_p$ texture. The small amount of plastic strain accommodated by the low volume fraction of primary alpha during rolling at 955°C [12] led to a slight "smearing" and rotation of the basal poles toward the TD direction, but not enough to noticeably eliminate the very strong RD component inherited from the unrolled material.

During high-temperature rolling without reheating, the temperature of the material dropped considerably toward the end of the rolling process [17]. Although the volume fraction of primary alpha did not change noticeably (Figures 2b, e), beta matrix decomposition occurred *during* rolling leading to a microstructure of primary alpha in a much stiffer transformed beta matrix. This microstructure increased the amount of plastic strain accommodated by $\alpha_p$ (relative

to that during rolling at 955°C with inter-pass reheating) and enhanced the formation in the $\alpha_p$ of a marked deformation texture comprising a strengthened texture component along the TD and the appearance of basal poles close to the ND (Figure 5b). Similarly, rolling at 815°C, at which the microstructure comprised a large amount of primary alpha and a small amount of beta, led to an increase in the intensity of the TD component, the disappearance of the RD component, and the appearance of the B-type texture for the $\alpha_p$ portion of the material (Figure 5c). These results confirm that the deformation of primary alpha contributes greatly to the formation of the B/T-type texture.

### 3.2.3 Secondary alpha texture

The $\alpha_s$ textures separated from the overall texture using the EBSD/EDS technique (limited to scan areas of 80 x 120 μm because of the size of the SEM chamber) shed further light on deformation during rolling with a preheat (furnace) temperature of 955°C. During rolling at 955°C with inter-pass reheating, most of the plastic strain was accommodated by the soft beta phase, and a strong deformation texture was formed in the beta. When the confounding influence of the primary alpha (and its associated RD texture component) was subtracted from the overall texture, the degree of variant selection during decomposition of the hot-worked beta became apparent (Figure 6a). Not surprisingly, the TD component was strongest in agreement with the work of Frederick [16]. However, additional weaker components along the RD and at 45° to the RD and TD, which are also related to the beta deformation texture, were evident.

The relationship between the $\alpha_s$ texture developed by hot rolling at 955°C with inter-pass reheating and the corresponding beta-deformation texture was further elucidated by a comparison of the basal pole figure for the $\alpha_s$ (figure 6a) and the (110) pole figure for the beta (Figure 7a). The beta texture was a classical "cube-on-face" type, i.e., (100)<011>. The correspondence of the locations of the intensity maxima on the two figures is evident, thus indicating that the burgers relation was obeyed for the close-packed planes in the beta and alpha phases during decomposition of the former. However, the comparison does show quantitative differences in the intensities at specific locations. The $(110)_\beta$ pole figure showed an essentially uniform intensity for all its texture components. On the other hand, the $(0001)_\alpha$ pole figure showed a stronger intensity along the TD and weaker intensities at the other locations. This difference in intensities can be explained by preferential variant selection during the beta-to-alpha transformation, for if all twelve variants of alpha phase were to occur with equal probability, the $(101)_\beta$ pole figure would be similar to the $(0001)_\alpha$ pole figure [14], which was not the case.

For hot rolling at 955°C without inter-pass reheats, part of the beta matrix decomposed to form $\alpha_s$ lamellae as the temperature dropped continuously during deformation and between passes. The deformation and transformation behavior therefore led to two distinct differences in the nature of texture evolution in comparison to the case involving reheating between passes. First, as noted in Section 3.2.2, the strain partitioned to the primary alpha was increased, thereby enhancing the formation of deformation texture in this constituent. Secondly, the beta deformation texture prior to transformation would have been sharper and the dislocation substructure developed in the beta phase would have been higher in samples rolled without reheating due to the reduced recovery rates at lower temperatures, let alone the absence of the reheating soak times. The very sharp $\alpha_s$ texture (Figure 6b) may thus be related to the sharp beta

deformation texture as well as a possible enhancement of the variant selection process associated with dislocation substructure.

Samples rolled at 815°C did not show any sign of $\alpha_s$ (Figure 3c, f).

### 3.3 Comparison of EBSD and XRD techniques

The overall textures determined by the "indirect" XRD technique (Figure 8) were similar to those derived via EBSD (Figure 4); i.e., they showed an increase in the intensity along the TD, a weakening of the intensity along the RD, and the appearance of titled ND basal poles as the rolling temperature was decreased. Although both techniques involved sampling of comparable areas, there were some distinctive differences in the measurements, especially for the sample rolled at 955°C with inter-pass reheating (Figure 4a and Figure 8a). In this case, XRD showed an extra texture component at 45° from the RD and TD. This component was most probably due to overlap of the alpha and beta peaks in the XRD patterns.

The XRD $\alpha_p$ textures (Figure 9), utilizing samples heated to the prior TMP temperature and furnace cooled to eliminate secondary alpha, were also similar, but not identical, to the corresponding EBSD data measured directly on the same samples (Figure 5). The XRD measurements revealed that rolling at lower temperatures caused an increase in the intensity of the TD component and a weakening of the RD component until it disappeared completely during rolling at 815°C, in broad agreement with the EBSD results. As surmised previously [6], some of the quantitative differences between the results from the two methods are a result of the contamination of the $(0001)_\alpha$ pole figures with $(101)_\beta$ peaks (e.g., Figure 7a).

The XRD $\alpha_s$-texture component calculated by subtraction of the $\alpha_p$ texture from the overall texture [9] (Figure 10) exhibited moderate basal-pole intensities along the TD that were similar to but lower in magnitude than those from the EBSD/EDS method (Figure 6). However, the weaker RD components were not detected by XRD. Hence, it is concluded that the XRD texture separation technique may yield results which are beneficial for overall process design but should not be viewed as being totally quantitative.

## 4.0 SUMMARY AND CONCLUSIONS

Samples of Ti-6Al-4V with an equiaxed-alpha preform microstructure were rolled with and without inter-pass reheating at high and low temperatures in the alpha + beta phase field. From this work, the following conclusions were drawn:

1. Irrespective of rolling temperature, the alpha-phase texture includes a component comprising basal poles along the TD. For high temperature rolling with inter-pass reheating, this is the main component and results from the formation of secondary alpha via non-random variant selection during the decomposition of the beta matrix.
2. High temperature hot rolling without reheating results in basal/transverse-type deformation texture with a weak basal component. The strength of the basal component increases by decreasing the rolling temperature.
3. Both primary and secondary alpha contribute to the basal/transverse type texture during low temperature rolling.
4. The presence of RD texture components following hot rolling may be associated with the persistence of a primary-alpha component present in the material prior to rolling.

## 5.0 REFERENCES


1. D. Eylon, S.R. Seagle, in: *Titanium 99: Science and Technology*, ed. I.V. Gorynin, and S.S. Ushkov, CRISM "PROMETEY", St. Petersburg, 2000, pp. 37-41
2. S.L. Semiatin, V. Smeetharaman, I. Weiss, in: *Advances in the Science and Technology of Titanium Alloy Processing*, ed. I. Weiss, R. Srinivasan, P.J. Bania, D. Eylon, and S.L. Semiatin, TMS, Warrendale, PA, 1997, pp. 3-73.
3. G. Lutjering, *Materials Science and Engineering* A243 (1998) 32-45.
4. M. Peters, G. Luetjering, in: *Titanium 80: Science and Technology*, ed. H. Kimura and O. Izumi, Kyoto, Japan, 1980, pp. 925-938.
5. G. Lutjering, J.C. Williams, in: *Titanium*, Springer-Verlag, Berlin, Germany, 2003, pp.220-224.
6. A.A. Salem, M.G. Glavicic, S.L. Semiatin, *Materials Science and Engineering A* (2008), in press.
7. M.G. Glavacic, J. D. Miller, S.L. Semiatin, *Scripta Materialia* 54 (2006) 281-286.
8. S.L. Semiatin and T.R. Bieler, *Metall. Mater. Trans.* 32A (2001) 1787-1799.
9. EDAX, Inc., 392 East 12300 South, Suite H., Draper, UT 84020.
10. Los Alamos Polycrystal Plasticity Code, Los Alamos National Laboratory, Report LA-CC-88-6, 1988.
11. S.L. Semiatin, S.L. Knisley, P.N. Fagin, F. Zhang, D.R. Barker, *Metall. Mater. Trans.* 34A (2003) 2377-2386.
12. S.L. Semiatin, F. Montheillet, G. Shen, and J.J. Jonas , *Metall. Mater. Trans.* 33A (2002) 2719-2727.
13. A.A. Salem, M.G. Glavicic, and S.L. Semiatin, submitted to *Materials Science and Engineering A* (2008).
14. J. Song, K. Hong, T.K. HA, H.T. Jeong, *Materials Science and Engineering* A449-451 (2007) 144-148.
15. W.G. Burgers, *Physica* 1 (1934) 561-586
16. S.F. Frederick, Report AFML-TR-73-265, 1973.
17. S.L. Semiatin, J.C. Soper, and R. Shrvpuri, *Metall. Mater. Trans.* 25A (1994) 1681-1692.
18. N. Gey, M. Humbert, M.J. Philippe, Y. Combres, *Materials Science and Engineering* A230 (1997) 68-74.

**Figure Captions**

Figure 1 SEM BSE images of the microstructure developed in the *unrolled* Ti-6Al-4V program material during heat treatment at 955°C for 4 hours followed by ((a) water quenching or (b) furnace cooling.

Figure 2 SEM BSE images of the microstructure developed in the Ti-6Al-4V program material via rolling at (a, d) 955$^{o}$C + 3 min reheat, (b, e) 955$^{o}$C + no reheat, and (c, f) 815$^{o}$C + 3 min reheat. The rolling direction (RD) is horizontal, and the transverse direction (TD) is vertical.

Figure 3 Alpha-phase (0001) pole figures determined by EBSD for *unrolled* Ti-6Al-4V heat treated 4 hours at 955°C followed by (a) furnace cooling or (b) water quenching. Texture contributions from the martensite phase in the water-quenched sample (b) were eliminated by *IQ*-partitioning. Scanned areas were 1.2 mm x 1.2 mm.

Figure 4 Alpha-phase ($\alpha_p$+$\alpha_s$) (0001) pole figures determined by EBSD for Ti 6Al-4V rolled *parallel* to the rolling direction of the as-received plate at (a) 955$^{o}$C + 3 min reheat, (b) 955$^{o}$C + no reheat, and (c) 815$^{o}$C + 3 min reheat or *perpendicular* to the rolling direction of the as-received plate at (d) 955$^{o}$C + 3 min reheat and (e) 815$^{o}$C + 3 min reheat. In all cases, RD corresponds to the rolling direction used in the specific rolling trial.

Figure 5 Primary-alpha ($\alpha_p$) (0001) pole figures determined by EBSD for Ti-6Al-4V rolled at (a) 955°C with 3-min inter-pass reheats, (b) 955°C with no reheating, and (c) 815°C with 3-min inter-pass reheats. Scanned areas were 20 mm x 15 mm.

Figure 6 Secondary-alpha ($\alpha_s$) (0001) pole figures determined by EBSD/EDS for Ti-6Al-4V rolled at (a) 955°C with 3-min inter-pass reheats and (b) 955°C without inter-pass reheats. The material rolled at 815°C with inter-pass reheating did not contain measurable secondary alpha. Scanned areas were 80 μm x 120 μm.

Figure 7 Texture of Ti-6Al-4V heat treated at 955°C for 4 hours and furnace cooled determined by the XRD technique: (a) Beta-phase (110) pole figure and (b) alpha-phase ($\alpha_p$+$\alpha_s$) (0001) pole figure.

Figure 8 Alpha-phase ($\alpha_p$+$\alpha_s$) (0001) pole figures determined by XRD for Ti-6Al-4V (a) rolled at 955°C with 3 min reheat, (b) rolled at 955°C without reheat, and (c) rolled at 815°C with 3 min reheat.

Figure 9 Primary-alpha ($\alpha_p$) (0001) pole figures determined by XRD for Ti-6Al-4V rolled at (a) 955°C with 3-min inter-pass reheats, (b) 955°C with no reheating, and (c) 815°C with 3-min inter-pass reheats.

Figure 10 Secondary alpha-phase ($\alpha_s$) (0001) pole figures determined by XRD texture subtraction technique [7] for Ti 6Al-4V (a) rolled at 955°C with 3 min reheat and (b) rolled at 955°C without reheat. Note, that the material rolled at 815°C with reheat did not have secondary alpha (Figures 2c, f).

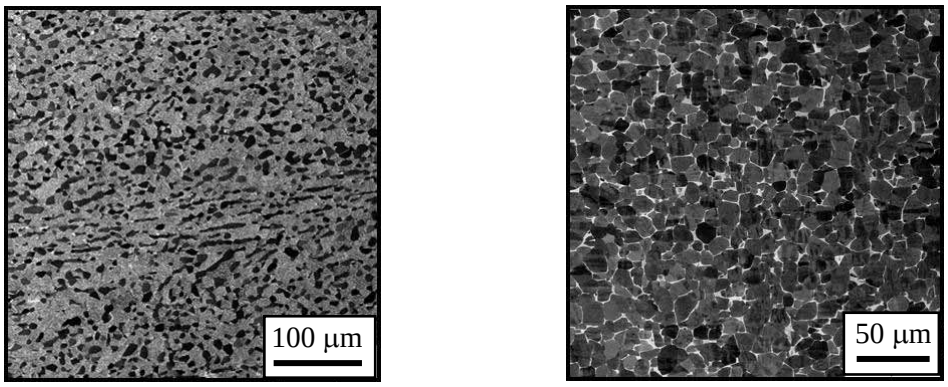


(a) (b)

Figure 1. SEM BSE images of the microstructure developed in the *unrolled* Ti-6Al-4V program material during heat treatment at 955°C for 4 hours followed by ((a) water quenching or (b) furnace cooling.

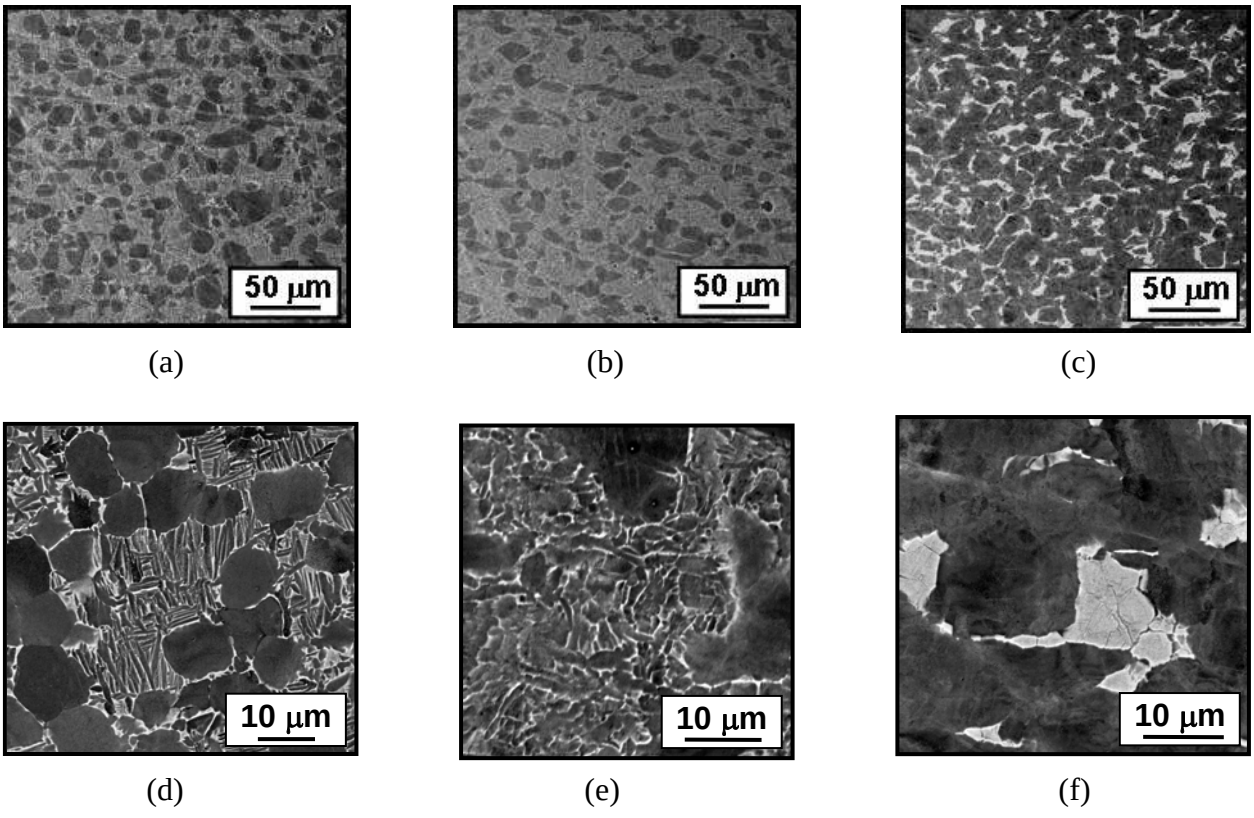


(a) (b) (c)

(d) (e) (f)

Figure 2. SEM BSE images of the microstructure developed in the Ti-6Al-4V program material via rolling at (a, d) 955$^{o}$C + 3 min reheat, (b, e) 955$^{o}$C + no reheat, and (c, f) 815$^{o}$C + 3 min reheat. The rolling direction (RD) is horizontal, and the transverse direction (TD) is vertical.

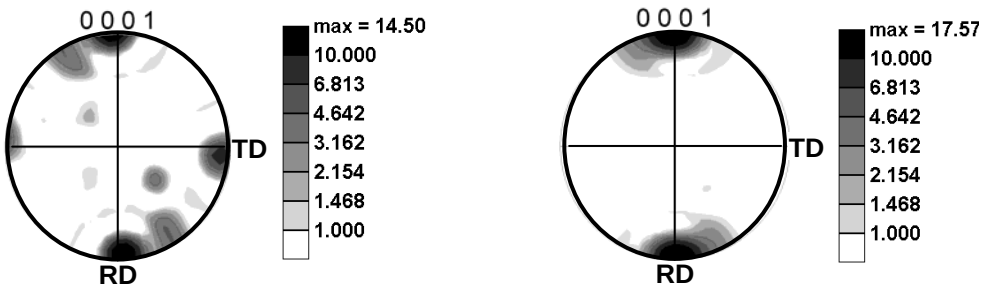


(a) (b)

Figure 3. Alpha-phase (0001) pole figures determined by EBSD for *unrolled* Ti-6Al-4V heat treated 4 hours at 955°C followed by (a) furnace cooling or (b) water quenching. Texture contributions from the martensite phase in the water-quenched sample (b) were eliminated by *IQ*-partitioning. Scanned areas were 1.2 mm x 1.2 mm.

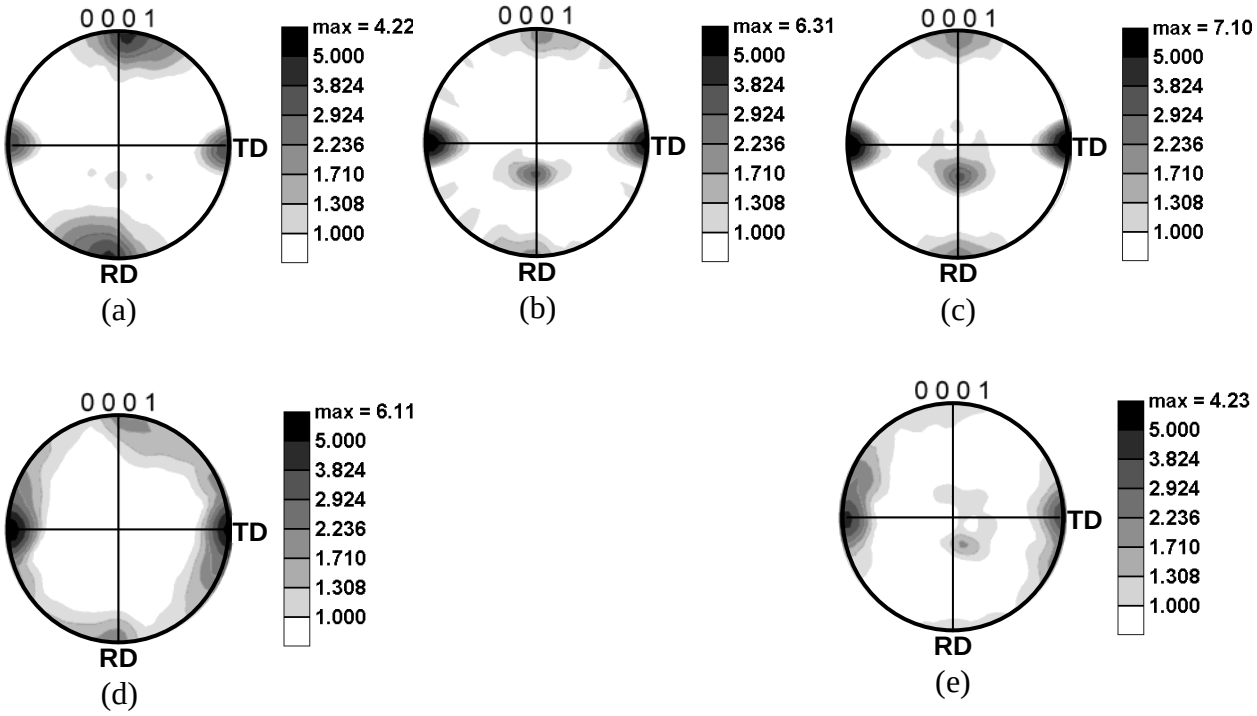


Figure 4. Alpha-phase ($\alpha_p+\alpha_s$) (0001) pole figures determined by EBSD for Ti-6Al-4V rolled *parallel* to the rolling direction of the as-received plate at (a) 955°C + 3 min reheat, (b) 955°C + no reheat, and (c) 815°C + 3 min reheat or *perpendicular* to the rolling direction of the as-received plate at (d) 955°C + 3 min reheat and (e) 815°C + 3 min reheat. In all cases, RD corresponds to the rolling direction used in the specific rolling trial.

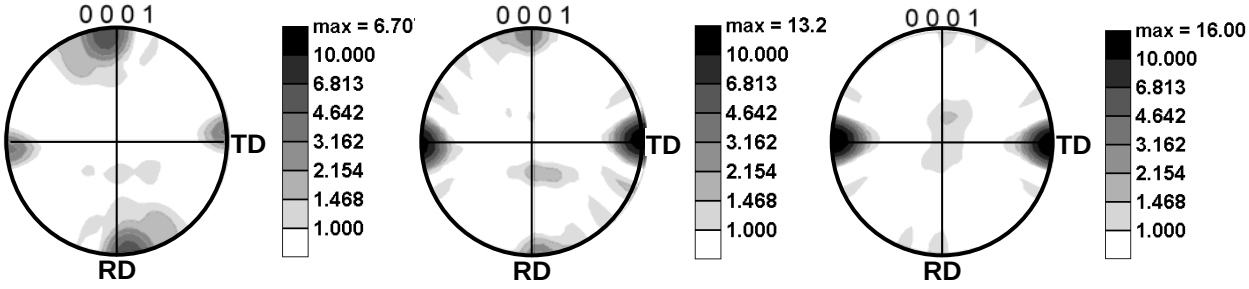


(a) (b) (c)

Figure 5. Primary-alpha ($\alpha_p$) (0001) pole figures determined by EBSD for Ti-6Al-4V rolled at (a) 955°C with 3-min inter-pass reheats, (b) 955°C with no reheating, and (c) 815°C with 3-min inter-pass reheats. Scanned areas were 20 mm x 15 mm.

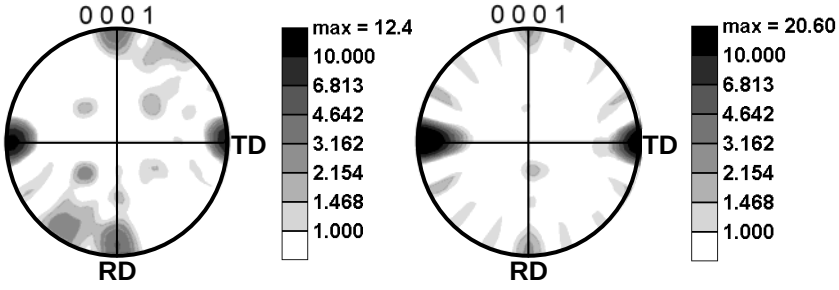


(a) (b)

Figure 6. Secondary-alpha ($\alpha_s$) (0001) pole figures determined by EBSD/EDS for Ti-6Al-4V rolled at (a) 955°C with 3-min inter-pass reheats and (b) 955°C without inter-pass reheats. The material rolled at 815°C with inter-pass reheating did not contain measurable secondary alpha. Scanned areas were 80 μm x 120 μm.

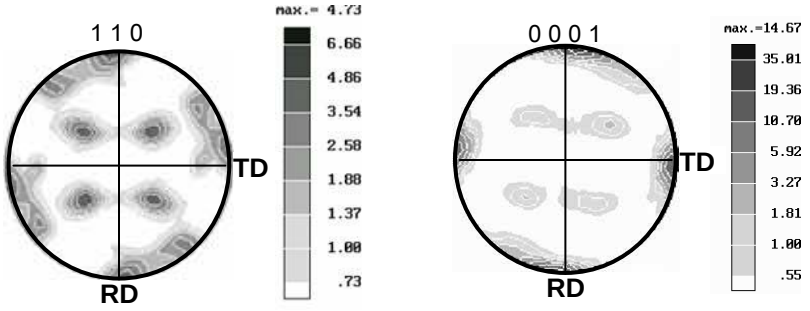


(a) (b)

Figure 7. Texture of Ti-6Al-4V heat treated at 955°C for 4 hours and furnace cooled determined by the XRD technique: (a) Beta-phase (110) pole figure and (b) alpha-phase ($\alpha_p$+$\alpha_s$) (0001) pole figure.

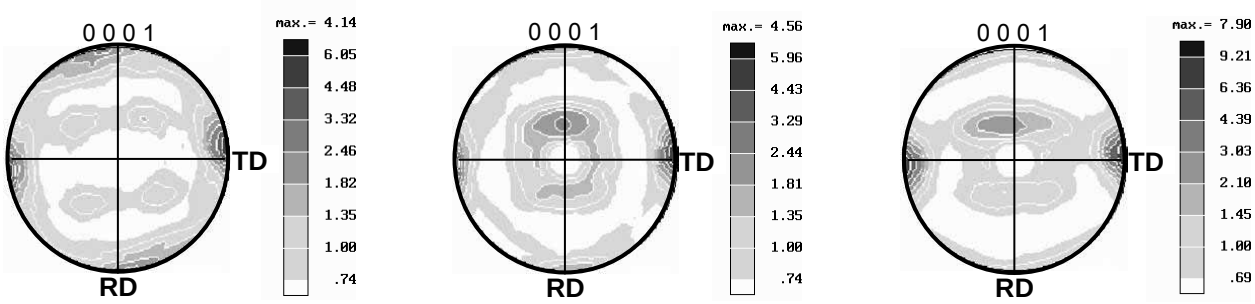


(a) (b) (c)

Figure 8. Alpha-phase ($\alpha_p+\alpha_s$) (0001) pole figures determined by XRD for Ti-6Al-4V (a) rolled at 955°C with 3 min reheat, (b) rolled at 955°C without reheat, and (c) rolled at 815°C with 3 min reheat.

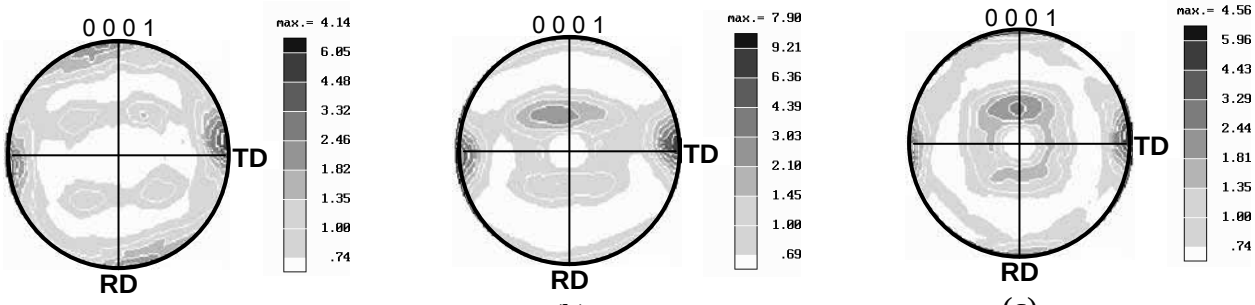


(a) (b) (c)

Figure 9. Primary-alpha ($\alpha_p$) (0001) pole figures determined by XRD for Ti-6Al-4V rolled at (a) 955°C with 3-min inter-pass reheats, (b) 955°C with no reheating, and (c) 815°C with 3-min inter-pass reheats.

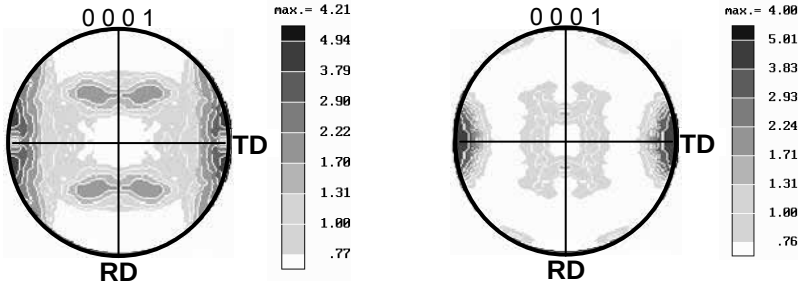


(a) (b)

Figure 10. Secondary alpha-phase ($\alpha_s$) (0001) pole figures determined by XRD texture subtraction technique [7] for Ti 6Al-4V (a) rolled at 955°C with 3 min reheat and (b) rolled at 955°C without reheat. Note, that the material rolled at 815°C with reheat did not have secondary alpha (Figures 2c, f).

# Hot deformation of Ti-6Al-4V single-colony samples

A.A. Salem[1,2,*] and S.L. Semiatin[1]

[1] Air Force Research Laboratory, Materials and Manufacturing Directorate,
AFRL/RXLM, Wright-Patterson AFB, OH 45433
[2] Universal Technology Corp., Dayton, OH 45432 USA

## Abstract

The hot deformation response of lamellar colonies of Ti-6Al-4V was established via uniaxial compression testing. For this purpose, samples with a rectangular cross section were cut from single colonies grown using a float-zone technique and then tested at 815°C. Each sample was oriented for single slip along one of seven different slip system in the alpha phase; i.e., one of the three <11**Error! Objects cannot be created from editing field codes.**0>{10**Error! Objects cannot be created from editing field codes.**0} (prism <a>), the three <11**Error! Objects cannot be created from editing field codes.**0>{0001} (basal <a>), or the <*c*+*a*> (pyramidal) systems was activated by orienting specific samples to have the highest Schmid factor on that particular system. Measurements of the critical resolved shear stress (CRSS) at yielding and the subsequent flow behavior revealed a strong dependence of mechanical behavior on colony orientation/activated slip system. The anisotropy in the CRSS and the tendency for flow softening at large strains was rationalized on the basis of the burgers orientation relationship between the alpha (hcp) lamellae and the beta (bcc) matrix and hence the orientation of alpha slip directions relative to those in the beta phase.

*Keywords*: Deformation mechanisms; Ti-6Al-4V; single colony; critical resolved shear stress; high temperature

## Acknowledgments

This work was conducted as part of the in-house research activities of the Metals Processing Group of the Air Force Research Laboratory's Materials and Manufacturing Directorate. The support and encouragement of the Laboratory management and the Air Force Office of Scientific Research (Dr. J. Fuller, program manager) are gratefully acknowledged. The yeoman assistance of J.M. Scott, P.N. Fagin, and F. Meisenkothen in conducting the experimental work is much appreciated. AAS was supported through Air Force Contract F33615-03-D-5801.

*Corresponding author. Tel:+1-397-255-1314; fax;+1-937-252-6373
E-mail address: ayman.salem@wpafb.af.mil (A.A. Salem)

## 1.0 INTRODUCTION

Providing an excellent combination of high strength, corrosion resistance, and low density, Ti-6Al-4V is the most commonly used alpha/beta titanium alloy. It accounts for approximately 80 pct. of the total titanium used in the US (Eylon and Seagle, 2000).

The mechanical behavior of Ti-6Al-4V depends on the microstructure and texture developed during thermomechanical processing (TMP) (Semiatin, et al., 1997; Lutjering, 1998). Depending on the specific TMP practice, one of three principal microstructures is commonly formed (Semiatin et al., 1997; Lutjering, 1998), namely, fully lamellar alpha, fully equiaxed alpha, and bi-modal (duplex). The fully lamellar and bi-modal microstructures both have lamellae of hcp alpha ($\alpha$) phase in a matrix of bcc beta ($\beta$) phase. The fully lamellar microstructure is formed during cooling from the beta field at a slow-to-medium rate; the lamellar-alpha phase and the beta matrix in which it grows follow a burgers orientation relationship (OR) in which $(0001)_\alpha$ is parallel to $(101)_\beta$ and **Error! Objects cannot be created from editing field codes.** is parallel to**Error! Objects cannot be created from editing field codes.** (Burgers, 1934).

Hot working processes in the $\alpha+\beta$ field (e.g., forging, extrusion, rolling, etc. at temperatures below the beta transus at which beta $\rightarrow$ alpha + beta) comprise the main approaches to breakdown the fully-lamellar microstructure and thus to obtain semi-finished billet and bar products with an equiaxed-alpha microstructure. The design of such processes relies heavily on quantitative descriptions of constitutive behavior and the microstructure changes which underlie plastic-flow behavior Although substantial progress has been made in understanding the constitutive response of single-phase titanium alloys, there has been comparatively less work conducted for two-phase alpha/beta Ti alloys.

The early work by Chan, et al. (1981) dealing with the room-temperature deformation of Ti-8Al-1Mo-1V with a colony-alpha microstructure represents one of the few efforts focusing on two-phase titanium alloys. In this research, compression testing of small samples cut from a plate material with a large grain/colony size revealed a marked anisotropy in the critical resolved shear stress for different prism <a>, basal <a>, and pyramidal <c+a> slip systems. Moreover, for a given type of slip system, Schmid's Law failed except for the specific case in which prism slip was activated parallel to the broad face the alpha lamellae (i.e., the alpha-beta interface). A similar anisotropy was reported during the room-temperature deformation of single colonies of Ti 5Al-2.5Sn-0.5Fe oriented for prism slip (Suri, et al., 1999). In this latter work, detailed TEM was used to correlate the observed anisotropy to the relative orientations of the slip vectors in the alpha and beta phases (Burgers, 1934; Welsch, et al., 1988; Suri, et al., 1999). In particular, Welsch, et al. and Suri, et al. demonstrated that only one of the three <a> slip directions in the alpha phase is closely aligned (within 0.7°) with a <111> slip direction in the beta phase, thus enabling easy slip transmission across the alpha-beta interface. The second <a> slip vector in the alpha phase had a misalignment of ~11.5° with the corresponding <111> slip direction in the $\beta$ phase, therefore resulting in more difficult slip transmission and a measurably higher critical resolved shear stress. The relative orientation of the third <a> slip vector in the alpha phase was even farther from a <111> slip direction in the beta phase. In follow-on work to that of Suri, et al., Savage, et al. (2001) determined the room temperature CRSSs of each of the prism <a> and basal <a> slip systems via micro-tension testing of single colonies of Ti-6242Si.

While the limited prior work on single colonies of alpha/beta titanium alloys has provided useful information on deformation behavior at room temperature, there appears to be no comparable single-colony results in the literature at hot working temperatures let alone at any temperature for the most commonly used two-phase alloy, Ti-6Al-4V. Therefore, the current work was undertaken to establish the slip-system anisotropy of the CRSS and stress-strain behavior for all six possible <a> slip systems and the <c+a> pyramidal slip system during hot working of Ti-6Al-4V. For this purpose, single colonies of Ti-6Al-4V were grown using a float-zone technique and subjected to uniaxial hot compression testing.

## 2.0 MATERIAL AND EXPERIMENTAL PROCEDURE

### 2.1 Material

Cylindrical Ti-6Al-4V bars containing large alpha/beta colonies were grown utilizing a vertical float-zone technique. The starting material comprised 12-mm diameter bars of Ti-6Al-4V with a measured composition (in weight percent) of 6.33 Al, 4.07 V, 0.19 Fe, 0.16 O, 0.01 C, 0.01 N, 0.0048 H, and balance Ti. Float-zone processing was performed under an argon atmosphere (partial pressure ~ 0.25 atm) in a Crystalox™ furnace. The float zone was produced via induction heating using a plate coil; bars measuring ~400-mm in length were rotated at a rate of 4 RPM and pulled through the hot zone at a speed of 2 mm/h. The colonies so grown ranged in length from 5 to 30 mm.

Thin foils parallel to $(0001)_\alpha$ were extracted from one of the rods to determine the precise orientation relationship between the alpha and beta phases via transmission electron microscopy (TEM) in a Philips CM200 $LaB_6$ microscope operated at 200 kV. The preparation of the TEM samples consisted of dimpled and ion milling to avoid the formation of hydride phases normally associated with electropolishing techniques.

### 2.2 Compression-sample preparation

Seven different colony orientations were chosen for compression testing. Each sample was fabricated to ensure the activation of single slip on the preselected slip system by maximizing the Schmid factor on that system. The samples were designated by the corresponding slip plane and slip direction (e.g., prism $a_1$). The seven IDs were thus denoted as prism $a_1$, prism $a_2$, prism $a_3$, basal $a_1$, basal $a_2$, basal $a_3$, and pyr (c+a) (Fig. 1). Furthermore, prism-slip samples had one face parallel to $(0001)_\alpha$, while basal-slip samples had one face parallel to a **Error! Objects cannot be created from editing field codes.** plane. Thus, samples oriented for prism slip had the basal plane parallel to the compression axis, thereby preventing slip on the basal plane. Samples aligned for basal slip had one prism plane parallel to the compression axis, therefore preventing slip on that plane. Pyramidal-slip samples had the compression axis perpendicular to the basal plane with a maximum misalignment between the c-axis and the loading direction of 2°. In this case, the loading direction was perpendicular to all three <a> burgers vectors, essentially eliminating the possibility of prism or basal slip along the close-packed direction.

The fabrication of the single-colony compression specimens (i.e., samples containing a single variant of alpha in a single crystal of beta) began by orienting small sections removed from the float-zone bars. The orientation operation was done using electron-backscatter diffraction (EBSD) in a Leica scanning electron microscope (SEM) operated at 20 kV and 10 nA. By this means, the crystallographic orientation of the alpha phase was determined simultaneously with the relative alignment of the beta phase, thus enabling the unambiguous identification of the three <11**Error! Objects cannot be created from editing field codes.**0> slip directions (Fig. 2). To facilitate the orienting process in the SEM, the single-colony sections of the Ti-6Al-4V bars were secured in a special fixture designed to fit inside the column. Subsequent to EBSD, the fixture was removed from the SEM and placed in a wire-EDM (electric-discharge machining) system that ensured minimal loss of sample alignment. A cut parallel to the basal plane in the alpha phase was then made using EDM.

After the basal-plane cut was completed, the orientation of the remaining material was confirmed using a Philips XRG Laue back-reflection x-ray system operated at 40 kV and 200 mA. The resulting Laue patterns were indexed using the OrientExpress™ software. The software was then used to estimate the rotations required to align the desired final sample orientation such that the desired slip-plane normal and slip direction both lay at 45° to the compression axis. The predicted rotations were then applied to the material using standard x-ray goniometers. Last, a Laue pattern was measured again and compared to the prediction for the desired orientation. After fine tuning of the orientation, final EDM cuts were made to produce a compression sample whose shape was a rectangular parallelepiped. Because of the limitation associated with the starting bar diameter and desired sample orientation, each finished specimen was relatively small. Typical sample dimensions were 3 x 3 x 5 mm with the loading axis aligned with the long side of the sample.

To remove the EDM recast layer and prepare the samples for testing, each specimen was ground flat by hand to a final grit size of 800 and then electropolished for two minutes in a solution of 10 ml perchloric acid and 90 ml methanol at –30°C using a DC power supply operating at 28 volts.

### 2.3 Test procedures

Uniaxial compression tests were conducted at 815°C using a servo-hydraulic testing machine outfitted with induction-heated titanium-carbide tooling. Prior to testing, samples were lubricated with glass, which also served to prevent oxidation. Each compression test was conducted at a constant true strain rate of -0.01 $s^{-1}$ to a final axial true strain of -0.15. Immediately after testing, samples were water quenched to retain the as-deformed microstructure.

Following testing, un-sectioned and sectioned samples were prepared for optical and SEM evaluation using standard metallographic procedures. Optical metallography and backscatter-electron (BSE) imaging (in a Leica SEM operated at voltage of 15kV and current of 8 nA) were both utilized to characterize the nature of slip and possible shearing of the alpha platelets and beta matrix.

The measured load-stroke data were reduced to resolved shear stress-resolved shear strain by converting first to true axial stress-strain and then applying Schmid's Law ($\tau = \sigma m_s$, in which $m_s$ represents the Schmid factor) and the strain-transformation equation.

## 3.0 RESULTS AND DISCUSSION

The key results of this investigation consisted of characterization of the as-grown single-colony Ti-6Al-4V samples and their flow behavior at 815°C.

### 3.1 Microstructure and crystallography of single-colony samples

EBSD of the as-grown single-colony samples revealed both the morphology and crystallographic orientation of the alpha platelets (Fig. 2). For example, one of the **Error! Objects cannot be created from editing field codes.** directions in the alpha platelets was indeed nearly parallel to the (broad) alpha-beta interface (inset in Fig. 2a). The corresponding $(0001)_\alpha$ , (11**Error! Objects cannot be created from editing field codes.**0)$_\alpha$ , and (10**Error! Objects cannot be created from editing field codes.**0)$_\alpha$ pole figures further quantified the orientation of each <a> slip direction relative to the sample coordinate system (Fig. 2b).

An overall picture of the morphology of the alpha and beta phases was also revealed in optical micrographs taken on an electropolished sample oriented for prism slip (Fig. 3). The front face of the sample containing the $(0001)_\alpha$ plane (which is parallel to $(101)_\beta$ plane) showed the alpha phase as thin platelets separated by interlayers of the beta matrix (Fig. 3a). The side and top faces of the sample revealed the finite breadth and length of the alpha platelets (Fig. 3b, c). The volume fraction of the alpha phase was ~0.90, and the average alpha-platelet thickness was ~ 8.5 μm (Fig. 2a). The beta interlayers were ~ 1-μm thick.

The orientation relationship (OR) between the alpha and beta phases in Ti-6Al-4V with a lamellar-alpha microstructure was revealed by TEM for imaging conditions in which the electron beam was parallel to $(0001)_\alpha \| (101)_\beta$ (Fig. 4a). Convergent-beam electron diffraction (CBED) patterns for both phases were superimposed on the bright-field (BF) TEM image with $[0001]_\alpha$ and $[101]_\beta$ zone axes (Fig. 4a). An analysis of the TEM images indicated that the OR between the alpha and beta phases in Ti-6Al-4V was indeed near that prescribed by the burgers orientation relationship and was in agreement with prior work for near-alpha titanium alloys (Mills, et al., 1998; Suri, et al., 1999; and Savage, et al., 2001).

Based on previous work, the OR was expected to result in one of the <a> slip directions in the hcp alpha phase ($a_1$ ~ **Error! Objects cannot be created from editing field codes.**) being parallel to one of the <111> slip directions in the bcc beta phase ($b_1$ ~ **Error! Objects cannot be created from editing field codes.**) (Fig. 4b). A careful examination of the SAD patterns revealed a slight misalignment of 0.8° about the $(0001)_\alpha \| (101)_\beta$ zone axes between the $a_1$ slip direction in the alpha phase and the $b_1$ slip direction in the beta phase (Fig. 4b). The $a_2$ slip direction in the alpha phase was misoriented by approximately 11.2° from the $b_2$ slip direction in the beta phase. The $a_3$ slip direction in the alpha phase was not close to any of the close-packed directions in the beta phase.

The relative inclination of the different slip directions to the alpha-beta interface was determined by overlapping the SAD patterns with the BF TEM image with $[0001]_\alpha$ and $[101]_\beta$ zone axes (Fig. 5). The measured inclinations of the $a_1$, $a_2$, and $a_3$ slip directions to the alpha-beta interface were 14.5°, 74.5°, and 45.5°, respectively.

## 3.2 Flow behavior

The flow behavior in terms of the resolved shear stress – strain plots revealed a number of interesting features for the samples cut to produce prism <a>, basal <a>, or pyramidal <c+a> slip.

### 3.2.1 Prism <a> deformation

Constant strain rate, resolved shear stress-strain data for the Ti-6Al-4V single-colony samples oriented for *prism* slip showed a significant anisotropy in both initial strength (~yield strength/CRSS) and subsequent strain-hardening behavior (Figure 6). The yield strengths for the prism $a_2$ and $a_3$ systems were ~35 pct. or 80 pct. higher, respectively, than that for prism $a_1$ slip. The different systems also exhibited different degrees of flow softening at large strains.

The anisotropy in the prism-slip mechanical behavior can be rationalized in the context of slip transmission across alpha-beta interfaces. For prism $a_1$ slip, for example, the slip vector in the alpha phase is closely aligned with a <111> slip direction in the beta phase phase. Consequently, dislocations can be transferred across the alpha-beta interface with minimum resistance (Suri, et al., 1999; Savage, et al., 2001).By contrast, a very high resistance for slip transmission across the interface was encountered by dislocations gliding on the $a_3$ system during testing of the corresponding prism sample because there was no closely-aligned <111> slip direction in the beta phase.. Consequently, the alpha-beta interface acted as a strong barrier to dislocation movement and increased the yield strength of the material. The small misalignment between the $a_2$ and $b_2$ directions (11.2°) resulted in a yield strength intermediate between those for the soft $a_1$ and hard $a_2$ prism slip systems. A similar behavior has been reported during the *room temperature* testing of near-alpha titanium alloys (Chan, et al., 1981; Suri, et al., 1999; Savage, et al. 2001). In particular, the observations for colonies 22 and 3 in the work by Chan, et al. (1981), colonies OA and OB in the work of Suri, et al. (1999), and the prism $a_1$ and $a_2$ samples in the work of Savage, et al. (2001) mirror the present results, even though the current tests were conducted at 815°C.

Despite the similarity in the relative flow stress of the prism systems at high temperature (present work) and room temperature (prior work), the large-strain behavior did show some noticeable differences. At room temperature, plastic flow at finite strains was characterized by an initial strain-hardening transient followed by steady-state flow. Not unexpectedly, a similar behavior was found for the easy-slip prism system ($a_1$) at 815°C. In contrast, the prism $a_2$ and $a_3$ systems showed marked or modest flow softening, respectively, following the initial strain hardening transient at 815°C. These latter behaviors may be ascribed to the difficulty of slip transmission when there are no co-linear slip vectors in the alpha and beta phases. Hence, as deduced for the hot working of poly-colony samples by Semiatin and Bieler (2001), the higher initial flow stresses and flow softening for the prism $a_2$ and $a_3$ systems are likely due to a Hall-Petch (H-P) like effect for the peak stress and the gradual loss of the H-P effect due to slip transmission at higher strains, respectively. The magnitude of the H-P contribution to the peak stress (at low strains) would depend of course on the inverse square-root slip length and the magnitude of the H-P constant. For a given alpha-platelet thickness, the slip-length contribution is greater for the $a_3$ system because its slip plane lies at a less shallow angle to the interface (~75°) than the $a_2$ system (~45°). However, the difference in inverse square-root slip length for the $a_2$ and $a_3$ slip systems for the present material (with relatively thick alpha plates) would be small. Thus, the major contribution to the difference in the peak stresses for prism $a_2$ and $a_3$

deformation was most likely related to the difference in H-P constants and the detailed nature of slip transfer in the two different cases.

Despite the hypothesis that slip transfer between the alpha and beta phases is inherently easy for the prism $a_1$ system and the fact that flow softening suggests slip transfer and the associated loss of H-P hardening for the $a_2$ and $a_3$ systems, metallography revealed no evidence of distinct slip steps following compression at 815°C. Specifically, numerous BSE SEM images did not reveal any shearing of the alpha-beta interfaces in deformed samples (Fig. 7) in contrast to the previous findings for room-temperature testing (Suri, et al., 1999; Savage, et al., 2001).

There are several possible explanations for the absence of slip steps in the present work. First, flow-localization calculations (Semiatin, 2000) suggest that the amount of strain concentration (leading to shear bands/slip offsets) is very low for deformations of the order of those imposed in the present work and strain-rate sensitivities typical of hot working at 815°C and a strain rate of 0.01 $s^{-1}$ (i.e., m ~ 0.15). In a similar vein, it has been shown that strains of the order of unity are required to *begin* dynamic spheroidization (due to platelet shearing) in Ti-6Al-4V with a polycolony microstructure containing coarse alpha plates (Shell and Semiatin, 1999). The high strain-rate sensitivity at hot-working temperatures contrasts with an m value which is very small at room temperature (m ~ 0). Hence, the strain localization process in the presence of a small thickness non-uniformity would be expected to occur very quickly (i.e., at rather low strains) at ambient temperature, as has been observed by Suri, et al. (1999).

In addition to the flow-localization argument, a small amount of migration of the alpha-beta interface during cool-down (due to the increase in alpha volume fraction with decreasing temperature) might have occurred despite the fact that the samples were water quenched after deformation. Such migration may have eliminated the interface roughness associated with slip transfer. Finally, the high deformation temperature and coarse alpha-plate thickness present in the float-zone samples may have allowed dislocation climb, dynamic recovery, and the formation of subgrains, thus minimizing the formation of the dislocation pile-ups that precede slip transmission.

### 3.2.2 Basal <a> and pyramidal <c+a> deformation

The mechanical behavior of samples oriented for basal <a> slip also showed a noticeable anisotropy (Fig. 8). However, the flow stress of the basal $a_1$ system was ~35 pct. *higher* than that for the basal $a_3$ system. Although the higher flow stress of basal $a_1$ compared to basal $a_3$ contrasts with the corresponding high-temperature observations for prism slip, the trend is very similar to that seen previously by Savage, et al. (2001) for room-temperature deformation via micro-tension testing. On the other hand, the room-temperature *compression* results of Savage, et al. (2004) did indeed show that the flow stress for basal $a_1$ slip was less than that for basal $a_3$ slip. Nevertheless, the room-temperature compression flow behavior of the basal $a_2$ system was close to that for basal $a_3$ which is similar to the findings in the current work (Figure 8).

Samples compressed parallel to the c-axis of the alpha phase showed the highest flow stress of all (Fig. 9, 10). In particular, the initial stress for <c+a> slip was more than twice that for the activation of prism $a_1$ slip, the softest system for Ti-6Al-4V.

## 4.0 SUMMARY AND CONCLUSIONS

A float-zone technique was used to produce Ti-6Al-4V bars with large lamellar colonies from which small single-colony compression samples were extracted. The alpha lamellae exhibited a classical burgers orientation relation with the beta matrix. Constant strain-rate compression testing of the single colony samples at 815°C revealed a distinct anisotropy in plastic-flow behavior. From this work, the following conclusions were drawn:

1. The CRSS for prism slip is lowest along the along $a_1$ direction and highest along the $a_3$ direction. The reverse is true for basal slip. The pyramidal <c+a> slip system had the highest CRSS of all. These trends are analogous to previous room-temperature observations for near-alpha titanium alloys with a lamellar microstructure.
2. Flow softening to various degrees was observed for all slip systems tested. It was most pronounced for pyramidal slip.
3. Shearing of beta lamellae due to slip transmission was not observed during high temperature deformation. This may be due to the small strains imposed and the sluggish kinetics of strain localization associated with high m values that characterize high-temperature plastic flow.

## 5.0 REFERENCES


1. Burgers, W.G., 1934. On the process of transition of the cubic-body-centered modification into the hexagonal-close-packed modification of zirconium, Physica 1, 561-586.
2. Chan, K.S., Wojcik, C.C., and Koss, D.A., 1981. Deformation of an alloy with a lamellar microstrucutre:Experiemental behavior of individual Widmanstatten colonies of an $\alpha$-$\beta$ titanium alloy, Metall. Trans. 12A, 1899-1907.
3. Eylon, D. and Seagle, S.R., 2000 in: Titanium 99; Science and Technology, CRISM "PROMETEY", St. Petersburg, pp. 37-41.
4. Laugier, J. and Bochu, date. OrientExpress$^{TM}$, Version 3.4, Laue software for Windows.
5. Lutjering, G., 1998. Influence of processing on microstructure and mechanical properties of ($\alpha$+$\beta$) titanium alloys, Mater. Sci. Eng. A243, 32-45.
6. Mills, M.J., Hou, D.H., Suri, S., and Viswanathan, G.B., 1998 in: Boundaries and Interfaces in Materials, TMS, Warrendale, PA, pp. 295-301
7. Savage, M.F., Tatalovich, J., Zupan, M., Hemker, K.J., and Mills, M.J., 2001. Deformation mechanisms and microtensile behavior of single colony Ti–6242Si, Mat. Sci. and Eng. A319–321, 398–403.
8. Savage, M.F., Tatalovich, J., and Mills, M.J., 2004. Anisotropy in the room-temperature deformation of $\alpha$-$\beta$ colonies in titanium alloys: role of the $\alpha$-$\beta$ interface, Phil. Mag. 84, 1127–1154.
9. Semiatin, S.L., 2000. Unpublished research, Air Force Research Laboratory, Wright-Patterson Air Force Base, OH.
10. Semiatin, S.L. and Bieler, 2001. The effect of alpha platelet thicjness on plastic flow during hot working of Ti-6Al-4V with a transformed microstructure, Acta Mater. 49, 3565-3573.
11. Semiatin, S.L., Seetharaman, V., and Weiss, I., 1997 in: Advances in the Science and Technology of Titanium Alloy Processing, TMS, Warrendale, PA, pp. 3-73.
12. Shell, E.B. and Semiatin, S.L., 1999. Effect of initial microstructure on plastic flow and dynamic globularization during hot working of Ti-6Al-4V, Metall. and Mater. Trans. 30A, 3219-3229.
13. Suri, S., Viswasnathan, G.B., Neeraj, T., Hou, D.-H., and Mills, M.J., 1999. Room temperature deformation and mechanisms of slip transmission in oriented single-colony crystals of an $\alpha$/$\beta$ titanium alloy, Acta Mater. 47, 1019-1034.
14. Welsch, G., Weiss, I., Eylon, D., and Froes, F.H., 1988 in: Sixth World Conference on Titanium, Societe Francaise de Metallurgie, Les Ulis Cedex, France, 1289-1293.

**Figure Captions**

Figure 1 Schematic illustration showing the relative orientation of the compression axis and the various slip systems in the present work: (a-c) prism <a> slip, (d-f) basal <a> slip, and (g) pyramidal <c+a> slip. The double line in a-c represents beta lamellae.

Figure 2 (a) EBSD inverse-pole-figure map for an as-grown single-colony sample (inset shows the orientation of the alpha unit cell) and (b) pole figures for this sample.

Figure 3 Optical micrograph showing the morphology of a single colony of Ti-6Al-4V oriented for prism <a> slip: (a) the front face of the sample is $(0001)_\alpha \| (101)_\beta$, (b) the top face (compression plane), and (c) the side face. The compression axis is vertical.

Figure 4 (a) Bright-field TEM image at the alpha-beta interface of a single-colony sample showing the adjacent beta and alpha lamellae. The insets are convergent-beam electron-diffraction patterns from the alpha and beta phases using $[0001]_\alpha$ and $[101]_\beta$ zone axes. (b) Selected-area diffraction pattern taken at the alpha-beta interface along the $[0001]_\alpha \| [101]_\beta$ direction revealing the relative alignment of the hcp (alpha-phase) $a_1$, $a_2$, and $a_3$ directions with bcc (beta) $b_1$ and $b_2$ directions confirming the near-burgers relation between the alpha and beta phases.

Figure 5 Bright field TEM micrograph and corresponding schematic drawing overlapped with the SAD results (with the beam direction parallel to $[0001]_\alpha \| [101]_\beta$) showing the relative inclination of the three <a> directions relative to the alpha-beta interface

Figure 6 Resolved shear stress-strain curves for Ti-6Al-4V single-colony specimens oriented to activate the prism $a_1$, $a_2$, or $a_3$ slip systems during compression at 815°C.

Figure 7 Backscatter-electron SEM image for a prism $a_1$ sample after compression at 815°C to a true strain of 0.12 followed by water quenching. No interface shearing was observed in the sample.

Figure 8 Resolved shear stress-strain curves for Ti-6Al-4V single-colony specimens oriented to activate the basal $a_1$, $a_2$, or $a_3$ slip systems during compression at 815°C.

Figure 9 Comparison of the resolved shear stress-strain curves for Ti-6Al-4V single-colony samples oriented to activate the pyramidal <c+a>, basal $a_1$, or prism $a_1$ slip system during compression at 815°C.

Figure 10 Comparison of all of the critical resolved shear stress (CRSS) data for basal <a>, prism <a>, and pyramidal <c+a> slip systems at 815°C.

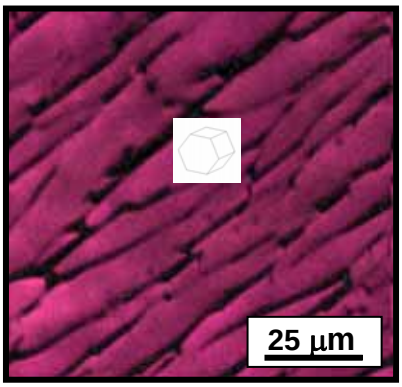


(a)

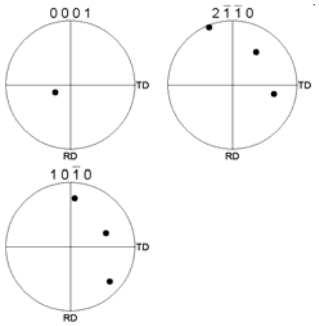


(b)

Fig. 1. (a) EBSD IPF map for as grown single colony with the inset revealing the orientation of the α phase and (b) the associated pole figures.

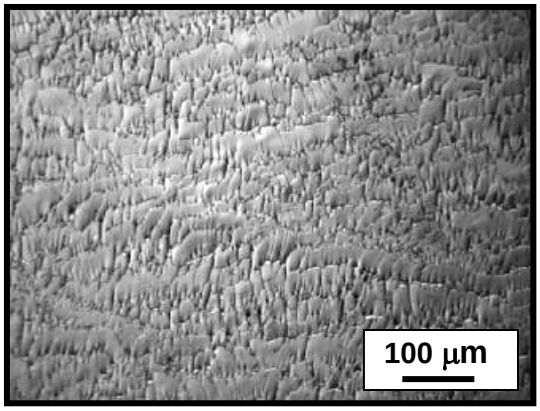


(b)

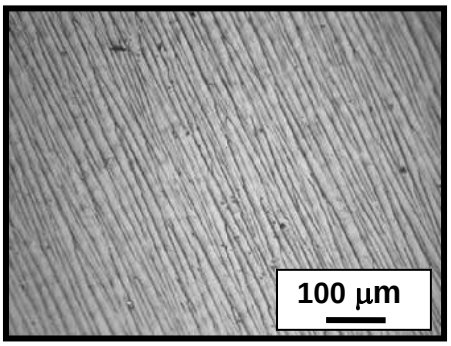


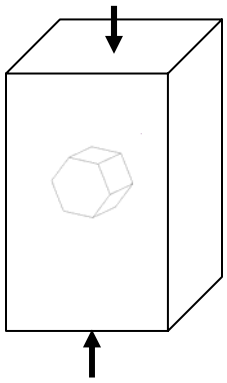

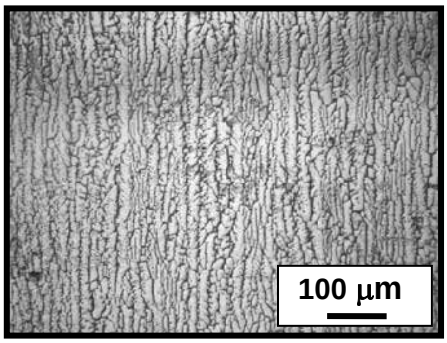


(a) (c)

Fig. 2. Optical micrograph showing the morphology of a single colony of Ti-6Al-4V oriented for prismatic slip. The front face of the sample (a) is $(0001)_\alpha \parallel (101)_\beta$. The top face (compression plane) (b) and the side face (b) shows the honeycomb morphology of the β phase. Compression axis is vertical

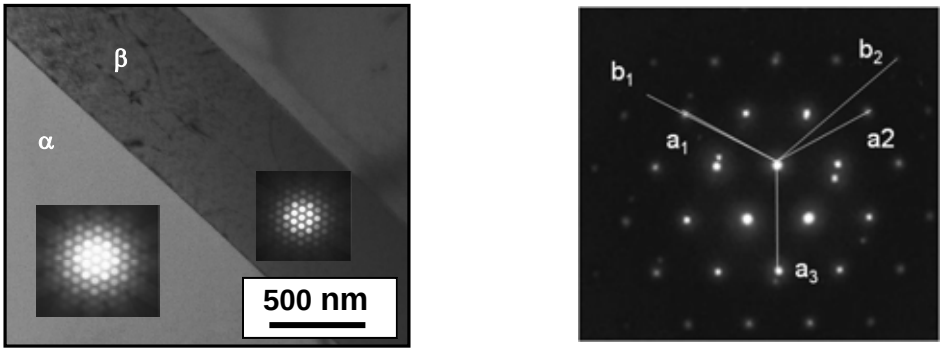


(a) (b)

Fig. 3. (a) Bright-field TEM image at the α-β interface showing a β-lamella surrounded by α-laths. Insets are convergent beam electron diffraction (CBED) patterns from the α and β phases using $[0001]_\alpha$ and $[101]_\beta$ zone axes. (b) Selected area diffraction pattern (SAD) taken at the α-β interface along the $[0001]_\alpha \| [101]_\beta$ direction revealing the alignment of the $\mathbf{a_1}$, $\mathbf{a_2}$, and $\mathbf{a_3}$ hcp directions with the $\mathbf{b_1}$ and $\mathbf{b_2}$ bcc directions confirming the near-Burger's OR between the α and β phases.

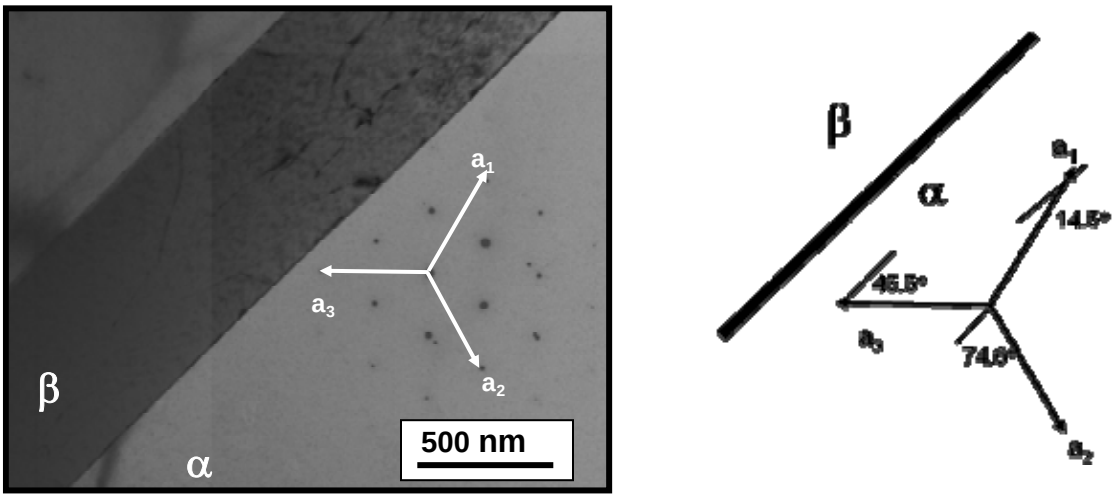


(a) (b)

Fig. 4. (a) Bright field (BF) TEM micrograph overlapped with SAD pattern with the beam direction parallel to $[0001]_\alpha \| [101]_\beta$ showing the relative orientation (b) of the three **a** directions relative to the α/β interface

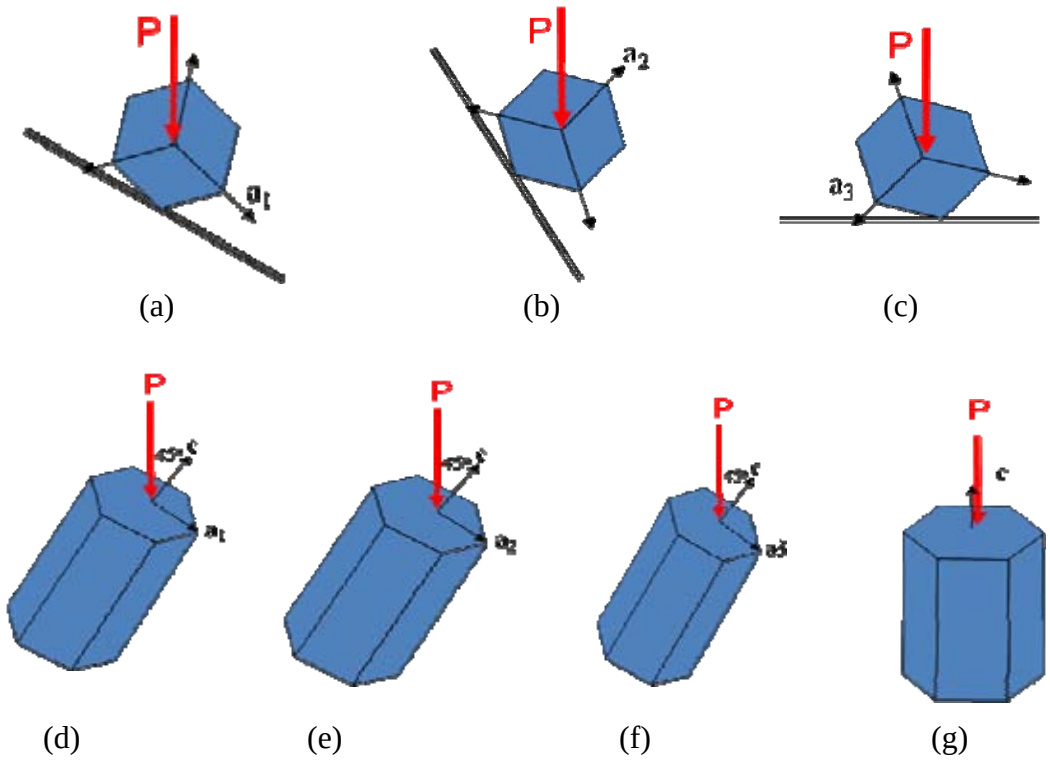


Fig. 5. Schematic showing the relative alignment of loading direction and each slips systems in each compression sample: (a-c) prismatic slip, (d-f) basal slip, and (g) pyramidal (c+a) slip. The double line in a-c represents β lamellae.

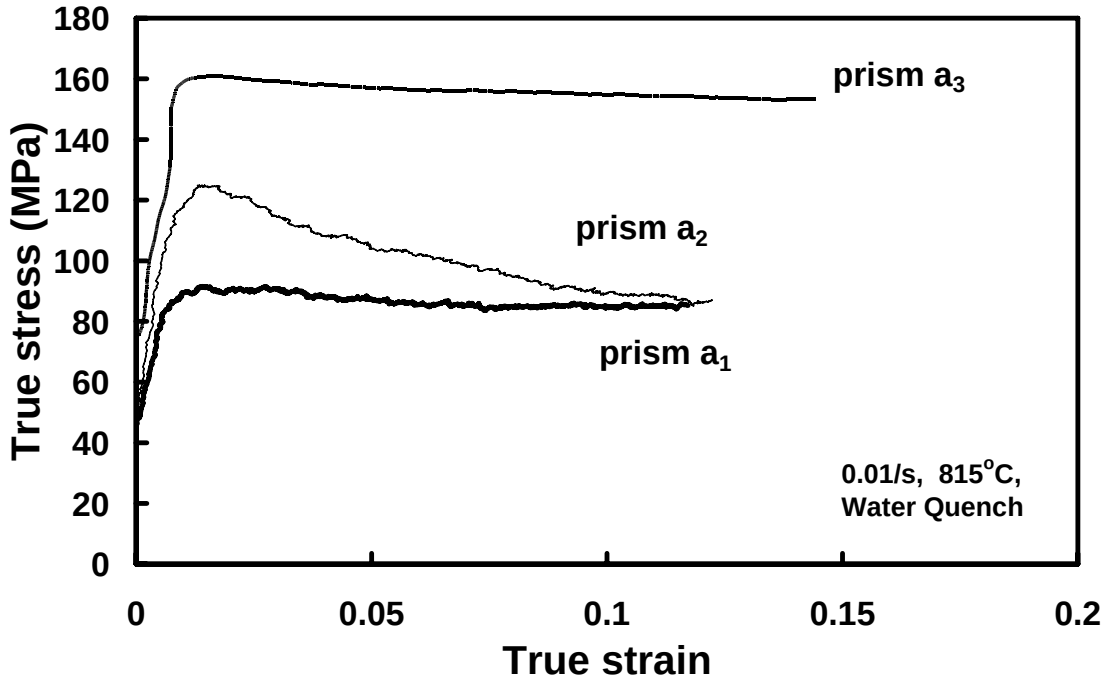


Fig. 6. True stress-true strain curves of Ti-6Al-4V single colonies oriented for prismatic slip at 815°C followed by water quenching.

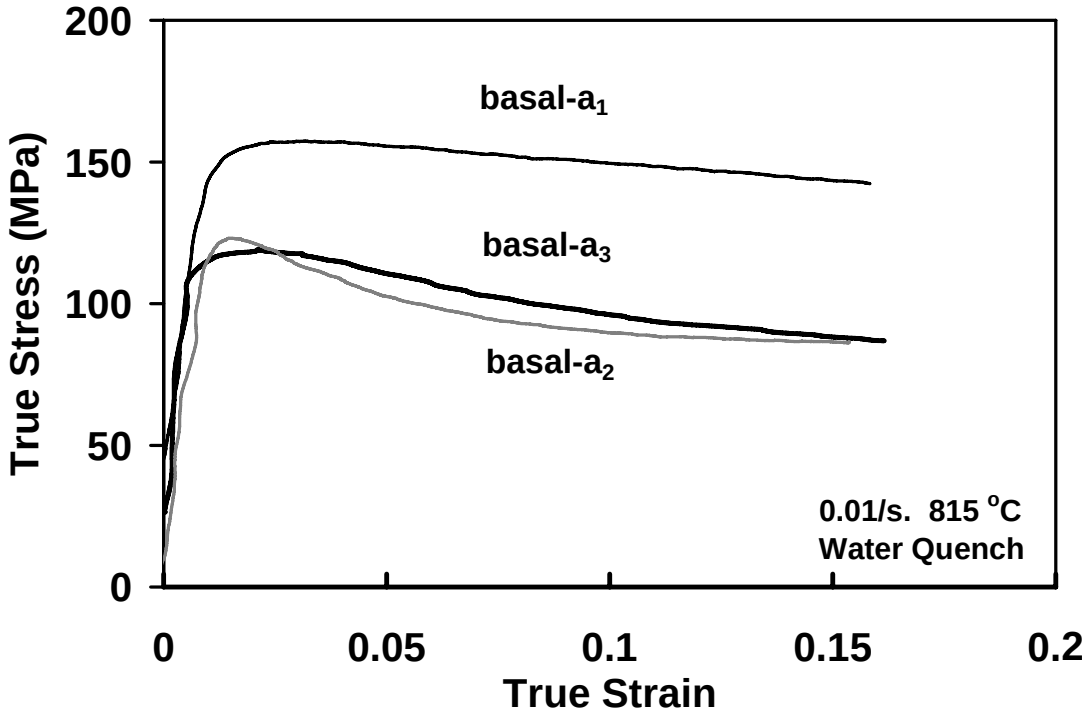


Fig. 7. True stress-true strain curves of Ti-6Al-4V single colonies oriented for basal slip at 815°C followed by water quenching.

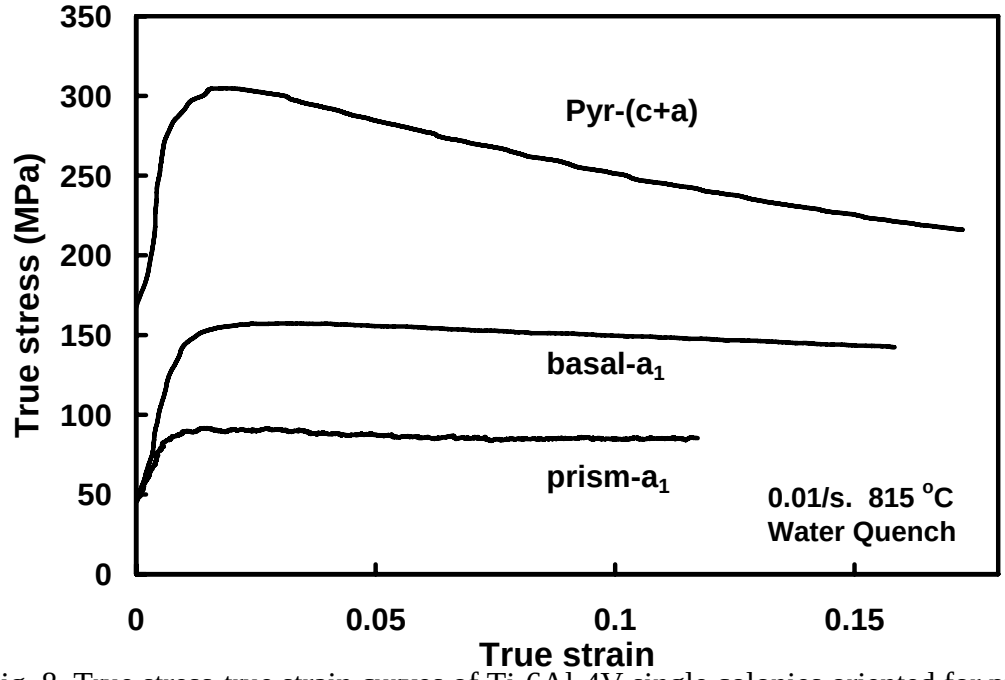


Fig. 8. True stress-true strain curves of Ti-6Al-4V single colonies oriented for pyramidal slip at 815°C followed by water quenching. Data for basal-$a_1$ and prism-$a_1$ were included for comparison.

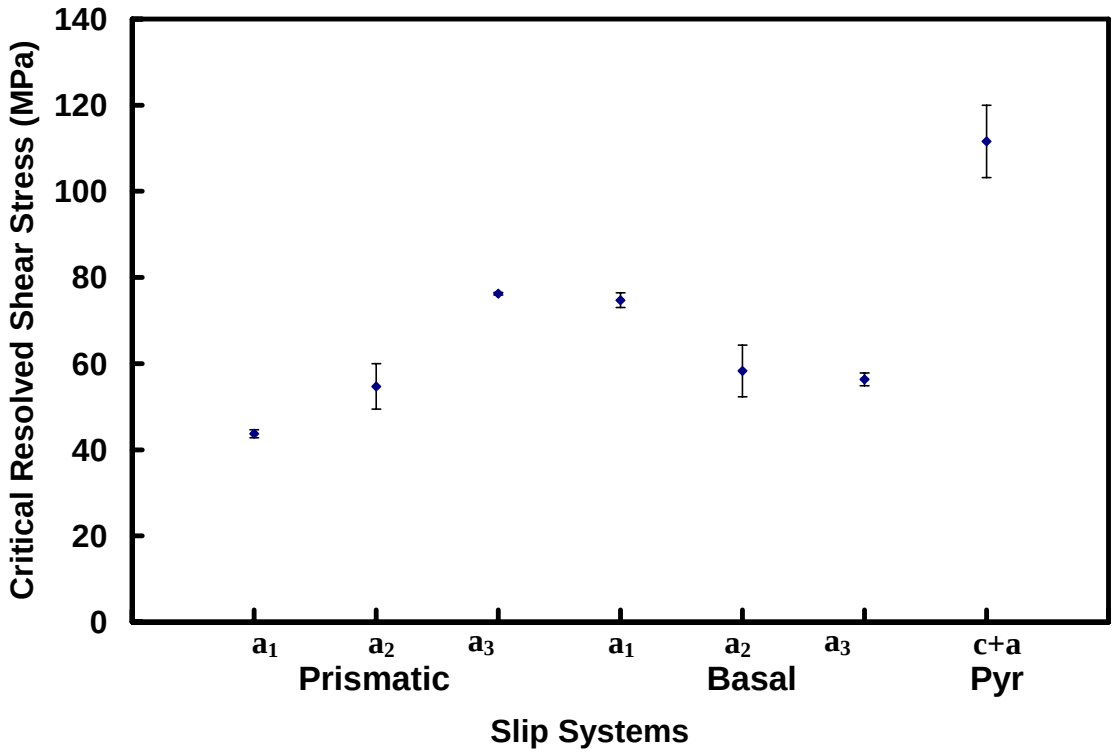


Fig. 9. Critical Resolved Shear stress (CRSS) for each basal, prismatic, and pyramidal slip systems at 815°C.

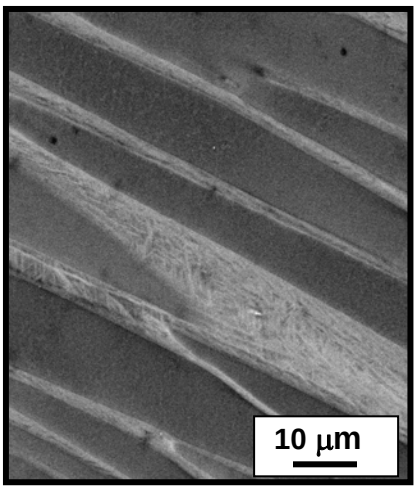


Figure 10. Back-scatter SEM image for prism-$a_1$ after compression at 815$^{o}$C to true strain of 0.12 followed by water quenching. No interface sharing was observed anywhere in the sample.